CHARACTERIZATION AND ASSESSMENT OF UNCERTAINTY IN SAN JUAN RESERVOIR, SANTA ROSA FIELD

A Thesis

by

ERNESTO JOSE BECERRA

Submitted to the Office of Graduate Studies of
Texas A&M University
in partial fulfillment of the requirements for the degree of

MASTER OF SCIENCE

December 2003

Major Subject: Petroleum Engineering

CHARACTERIZATION AND ASSESSMENT OF UNCERTAINTY IN SAN JUAN RESERVOIR, SANTA ROSA FIELD

A Thesis

by

ERNESTO JOSE BECERRA

Submitted to Texas A&M University
in partial fulfillment of the requirements
for the degree of

MASTER OF SCIENCE

Approved as to style and content by:

W. John Lee (Chair of Committee)	Duane McVay (Member)
Robert R. Berg (Member)	Hans Juvkam-Wold (Head of Department)

December 2003

Major Subject: Petroleum Engineering

ABSTRACT

Characterization and Assessment Uncertainty in San Juan Reservoir- Santa Rosa Field.

(December 2003)

Ernesto José Becerra, B.S., Universidad de Los Andes, Venezuela

Chair of Advisory Committee: Dr. W. John Lee

This study proposes a new, easily applied method to quantify uncertainty in production forecasts for a volumetric gas reservoir based on a material balance model (p/z vs. G_p). The new method uses only observed data and mismatches between regression values and observed values to identify the most probable value of gas reserves. The method also provides the range of probability of values of reserves from the minimum to the maximum likely value. The method is applicable even when only limited information is available from a field. Previous methods suggested in the literature require more information than our new method.

Quantifying uncertainty in reserves estimation is becoming increasingly important in the petroleum industry. Many current investment opportunities in reservoir development require large investments, many in harsh exploration environments, with intensive technology requirements and possibly marginal investment indicators.

Our method of quantifying uncertainty uses *a priori* information, which could come from different sources, typically from geological data, used to build a static or prior reservoir model. Additionally, we propose a method to determine the uncertainty in our reserves estimate at any stage in the life of the reservoir for which pressure-production data are available.

We applied our method to San Juan reservoir at Santa Rosa Field, Venezuela. This field was ideal for this study because it is a volumetric reservoir for which the material balance method, the p/z vs. G_p plot, appears to be appropriate.

DEDICATION

To Ernesto José, Juan José and Maria José who are my inspiration and motivation. They are such precious treasures, who give me light and feed my soul.

To my wife, Miriam Celina with all my love. She supports me in all my endeavors; she also feeds my soul with her knowledge and precious life.

To my family for their love and continuous support. They always believe in me. To all of them, thanks a lot.

ACKNOWLEDGEMENTS

First of all, I want to thank God for giving me a life full of love and happiness.

My gratitude goes to my family and my wife's family for their love and support.

A special thanks to Dr. W. John Lee for receiving me in his research group and sharing his experience and good advice with me.

I appreciate the cooperation and support that Dr. Duane McVay gave me. This research would not have been possible without his contribution.

I also want to express my gratitude to Dr. Robert R. Berg for being part of my committee.

I acknowledge those people from the Venezuelan Student Association who have been like a family during our stay in College Station. I also want to thank my classmates who have shared their experiences and cultures with me.

I would like to thank PDVSA for their cooperation and for sponsoring my study at Texas A&M University.

Last but not least, I wish to thank my wife, Miriam Celina, for her support and unlimited belief in me.

TABLE OF CONTENTS

LIST OF FIGURES

FIGURE Page

LIST OF TABLES

Page

CHAPTER I
INTRODUCTION

Overview

Uncertainties complicate our decisions in the petroleum industry. For example, although we know that in any reservoir model an uncountable number of factors affect the most likely realization, reservoir management decisions are often based on predictions from a single realization of a calibrated reservoir model.

To assess the effects of uncertainty, we sometimes resort to studies of the sensitivities of predictions to values of parameters that are of key importance in the model. However, to make a formal and complete estimation of uncertainty, we need a full range of the distribution of the forecasted variable. One could wonder why we complicate things with concern about uncertainty if, historically, our managers have handled the majority of decisions simply by choosing the single scenario most likely to be successful. The answer is that, two or three decades ago, the margin of profit in the petroleum industry was large enough to overcome high production costs and inappropriate investments, which in some cases were associated not only with substandard operational practices but also with a sub-optimal development plan. For a highly profitable business, it was unnecessary to measure the range of uncertainty. Today, with potential narrow profit margins, we need a clear picture of variability of our investments.

To quantify the effects of uncertainty, some diverse approaches have been described in the literature. A common method simply sums the probability-weighted net present values of all possible outcomes value (expected monetary value). Other, more complex, methods seek to estimate uncertainty with its respective ranges. An example of these more complex methods was presented by Floris *et al.*[1] In this paper, the authors presented several methods that assess uncertainty in different ways. Floris *et al.* focused

---

This thesis follows the style of the *Journal of Petroleum Technology.*

their attention on quantification of the production forecast. They asked different research groups to estimate uncertainty in a production forecast from a synthetic case study. Although each group analyzed the same data, the uncertainty ranges they reported were quite different, and appeared to depend on the method that each group used. Floris *et al.* called this study the production forecast uncertainty quantification or PUNQ exercise.

McVay *et al.*[2] analyzed the PUNQ results and other treatments of uncertainty in the literature, and noted the confusion that arises between the reduction of uncertainty in and the precision of a production forecast. McVay *et al.* noted that forecasts with narrow ranges of uncertainty reported are not necessarily more accurate (i.e., closer to the"truth") than other forecasts with much wider ranges of uncertainty. McVay *et al.* also noted that, while the true value of future production lay outside the range of uncertainty some participants obtained in the PUNQ exercise, this does not necessarily mean that the methods these participants used are not valid for the estimation of the range of certainty. Instead, this underestimation of the range of uncertainty could be due to lack of data and lack of knowledge about the area under study. McVay *et al*. concluded that a fundamental problem with existing methods is that is no way to verify their trustworthiness. McVay *et al*. proposed to try to calibrate the method used to estimate uncertainty with previous data to improve the reliability of future calculated ranges of uncertainty.

Nepveu[3] presented an interesting approach based on Bayesian inversion with special application to cases where only limited data are available. Egberts *et al.*[4] presented an uncertainty quantification based on the maximum entropy method. Their method requires many different realizations of the reservoir that reproduce the historical data with satisfactory accuracy.

In our study, we will examine the Santa Rosa Field, located in the northern part of the eastern Venezuela Basin[5] (**Fig. 1.1**). This small gas reservoir covers 1636 acres and is one of the fields of the greater Anaco area. Gas production is obtained from the Cretaceous sequence consisting of the San Antonio and San Juan formations.

Bottomhole pressure analysis has confirmed the pressure separation of the Lower San Juan - San Antonio reservoir from the Upper San Juan reservoir. The Santa Rosa Field produces from the Upper San Juan reservoir at depths ranging from 9,600 feet (sub-sea) at the crest of the structure to 12,500 feet (**Fig. 1.2**)[6]. The gas trap on top of the reservoir is provided by the limestone-shale in the overlying the Merecure formation. The San Juan reservoir was discovered in 1969, and initiated its production in June, 1973 when well RG134-8 was completed as a gas producer.

The upper part of the San Juan formation is uniform in the Anaco region. It consists of a deltaic system comprising mostly sandstone with scattered shale. This reservoir is limited between the Cretaceous and the Oligocene (**Fig. 1.3**). A typical log from the reservoir is shown in (**Fig. 1.4**)[7].

Fig. 1.1 – Location of the San Juan reservoir of the Santa Rosa field, eastern Venezuela (after ref. 5).

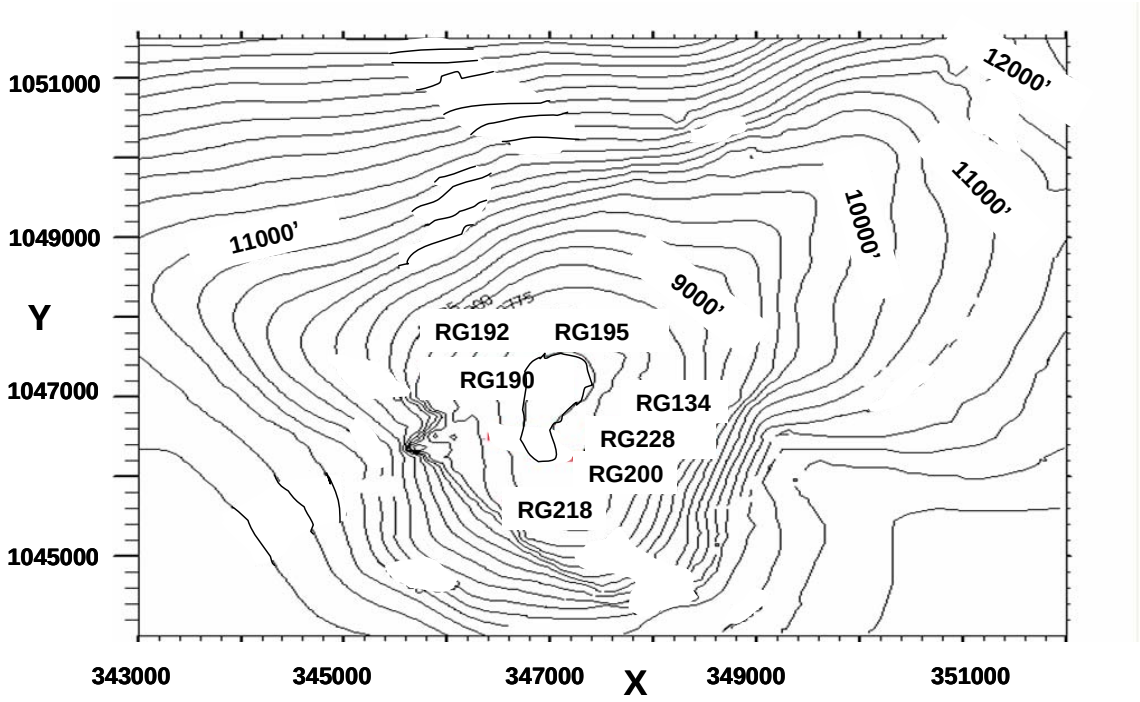

Fig. 1.2 – Structure map, top of San Juan Reservoir in Santa Rosa Field.

Because of the importance that gas has achieved in the Venezuelan economy, the government reactivated this gas reservoir, which had been considered to be marginal, and had not been included as a priority in the country's development plan.

This reservoir has been classified as a gas condensate reservoir because of substantial liquid production, but it is adequately modeled as a wet gas reservoir, with single-phase gas flow in the reservoir. The maximum liquid saturation from condensation in the reservoir is less than 2 percent (43 °API at 60 °F) according to a bottomhole reservoir fluid sample that was taken in Well RG190-2. The dominant drive mechanism is solution-gas expansion. The original gas in place (OGIP) is estimated to be 2.93 $x10^8$ MSCF, and the cumulative production has reached 1.37 $x10^8$ MSCF, a recovery efficiency of about 47 percent to date.

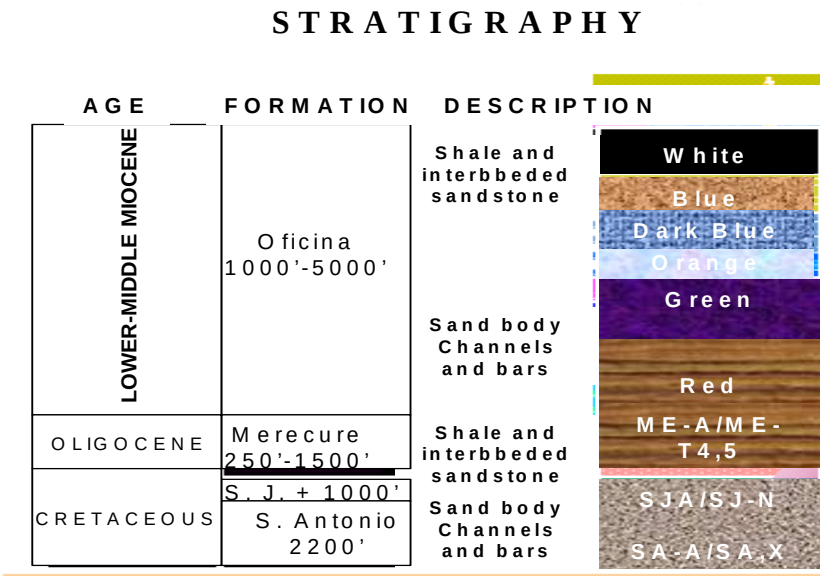

Fig. 1.3 –Stratigraphic column, Santa Rosa sequences, Anaco region (after ref. 7).

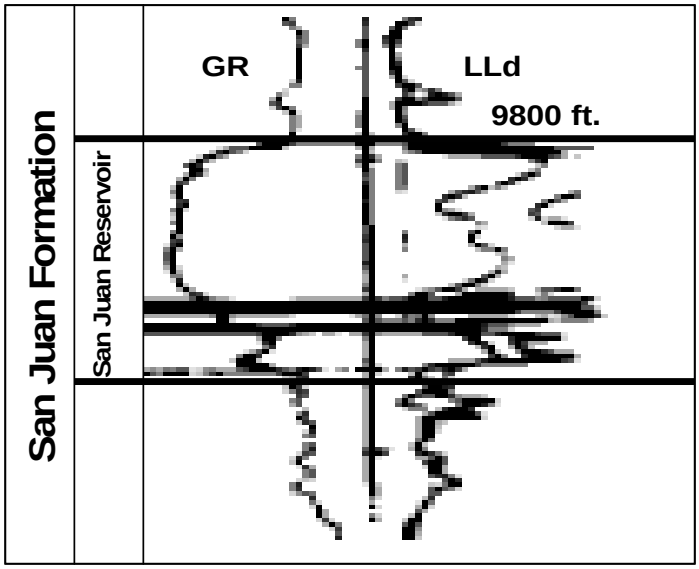

Fig. 1.4 –Typical log for San Juan reservoir gas (after ref. 7).

To study this field, we must analyze all available data. For reservoir simulator studies discussed in the Appendix, core and well log data are available to allow us to distribute

reservoir properties across the field. Pressure and production histories are required in both material balance and simulator studies. A volumetric estimate of original gas in place is available.

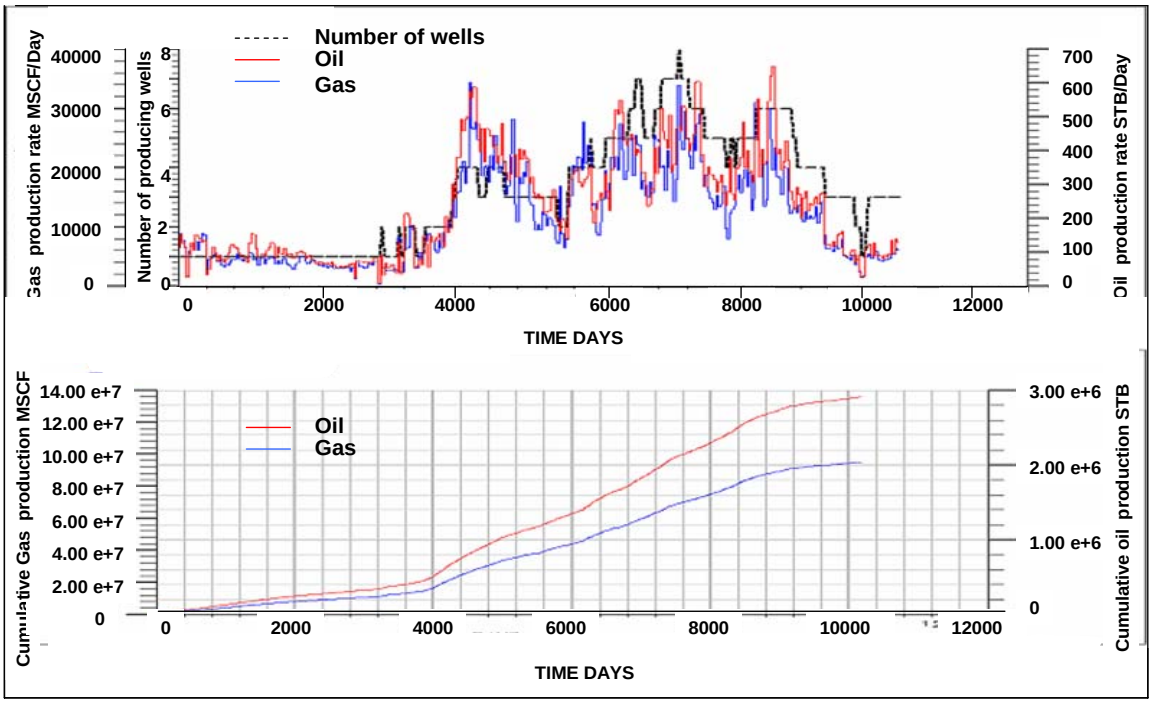

Fig. 1.5 – Production history of San Juan reservoir, Santa Rosa Field.

Status of the Problem

In current operations, profit margins are not large enough to overcome the drag of high production costs in mature and marginal reservoirs. In some cases, these high production costs are associated with a sub-optimal development plan as well as poor operational practices. Poor operational practices can be remedied with a careful and

deliberate plan to minimize operational costs, but a proper choice of development plans can require a realistic assessment of uncertainty. Specifically, in the San Juan reservoir, with its narrow margin between operational cost and revenues, it is important to estimate accurately or to at least be aware of the risks to avoid unfortunate investments.

San Juan is a mature gas field that has been producing for more than 27 years. Production reached its peak after 22.5 years of production when six wells were producing. Since then, gas and oil production rates have steadily declined, as shown in **Fig. 1.5.** Currently only three wells are producing, and current rates are 3,600 Mscf/D of gas, 25 STB/D of oil, and 20 STB/D of water. Gas recovery is about 47 percent of the original gas in place. Additional recovery of 42 percent (for an ultimate recovery of 89 percent) appears quite feasible using a detailed reservoir description and a better understanding of reservoir performance to optimize the reservoir development plan.

The major barrier to developing an optimal operating plan for the San Juan reservoir is the lack of characterization due to the limited data available, including limited shut-in pressure data that are surrogates for "local" average reservoir pressures. Although this reservoir has been producing for about 27 years, few studies have been performed on the reservoir. PDVSA conducted three studies, including a geological description and studies of operational and production practices. To add to the difficulties in understanding the field, some mechanical problems are explained poorly in the well files.

Objectives

The broad objective of his research is to provide a calibrated reservoir model as a tool to forecast reservoir performance. However, the major new development in this effort is to develop a method to assess uncertainty in reserves and in production forecasting starting with information available in the earlier stages of reservoir development. Specific objectives include the following:

- Develop a calibrated reservoir model that will be a tool to forecast future performance.
- Develop a methodology to readily calibrate the geological model.
- Assess uncertainty in reserve estimation.
- Identify how the range of confidence in reserve estimates changes with time from early to late times in the history of the San Juan reservoir.

Procedure

We will use the following general procedure to reach our research objectives.

- We will review a volumetric estimate of gas in place.
- We will apply material balance methods to develop a preliminary estimate of the reservoir size, and to assess the possibility of external sources of energy, such as a water drive.
- Starting with the earliest reported pressure and production data, we will assess uncertainty at each time new pressure and production data are available.
- We will model the reservoir using a black-oil simulator even though, strictly speaking, the reservoir fluid is a gas condensate.
- We will construct a one-cell model to perform dynamic material balance calculations that will allow us to assess uncertainties in reserves and production forecasting.
- We will construct a multi-cell model to generate a more complete calibrated model to use to forecast future reservoir performance and serve as the basis for conclusions and recommendations regarding a reservoir development plan.

The preceding general procedure will be implemented using the following steps:

1. Collect and review the data needed to construct a reservoir model. As necessary, we will review, organize and finally reduce them to a form usable in a numerical simulator.
2. Calculate gas in place using pressure and production history and the material balance model. We will compare this estimate with the volumetric estimate available.
3. Estimate OGIP, reserve and assess uncertainty at each time new pressure and production data are available.
4. Construct a one-cell model static model of the reservoir, and use this model in a reservoir simulation to fine tune the reservoir description from the material balance analysis.
5. Construct a three-dimensional static model of the reservoir, and use the model as the basis for a dynamic model that simulates reservoir depletion on a field-wide scale.
6. Identify and report our results, conclusions, and recommendations.

Importance

The importance of this research is that it will provide a general view on how to assess uncertainties in early stages of model calibration using *a priori* (volumetric) and updated reservoir data. The research will allow us to determine how uncertainty changes as more data become available. In addition, the research results will provide an excellent tool to minimize the impact of uncertainties in reservoir development.

CHAPTER II
METHODOLOGY

In summary, our approach was (1) to examine data from the San Juan reservoir from geological studies (volumetric estimate), (2) perform a material balance (p/z plot) study, in which we examined change in uncertainty in reserves estimates as more data became available, (3) refine the material balance model with a single-cell reservoir simulator model, and (4) refine the reservoir description even more with a multi-cell reservoir simulator model.

In the material balance work, we first verified that the reservoir is a volumetric accumulation with no pressure support from an aquifer. The p/z vs. cumulative gas production, G_p, plot for all available data (**Fig. 2.1**) supports this hypothesis and also provides an estimate of original gas in place to compare with volumetric estimates. **TABLE 2.1** presents the pressure-production data used in this analysis.

TABLE 2.1 – PRODUCTION DATA, SAN JUAN RESERVOIR

Date	Pressure	Z	P/Z	G_p	N_p	^oAPI	γ	GE	G_{pt}
	psia		psia	MMscf	MMstb		Oil	MMscf	Mscf
15/12/72	4679	1.0194	4590	0	0.00	44.30	0.805	0.00	0.00
31/08/81	3788	0.9612	3941	14987	0.22	44.40	0.804	142.48	1.51E+07
1/4/1982	3606	0.9522	3787	16018	0.24	45.30	0.800	155.58	1.62E+07
1/11/1984	3979	0.9522	4179	28664	0.42	46.40	0.795	283.49	2.89E+07
30/11/84	3984	0.9522	4184	29671	0.44	46.40	0.795	292.78	3.00E+07
30/11/84	3736	0.9522	3924	29671	0.44	46.11	0.797	291.25	3.00E+07
30/09/89	3575	0.9511	3759	70412	1.08	47.30	0.791	731.33	7.11E+07
13/02/01	2396	0.9184	2609	135509	2.06	47.60	0.790	1407.54	1.37E+08
16/02/01	2079	0.9171	2267	135509	2.06	47.00	0.793	1391.03	1.37E+08
10/4/2001	2476	0.9194	2693	135911	2.06	47.50	0.791	1409.81	1.37E+08

Cumulative oil production, N_p, is actually condensate, which was converted to gas equivalent in Table 2.1 and produced gas. The conversion is based on the following considerations:

$$G_{pt} = G_p + GE \cdot N_p \quad \text{(1)}$$

G_p is the produced gas, while gas equivalent, GE, is calculated from

$$GE(scf / STB) = 133{,}000 \cdot \frac{\gamma_o}{PM_o} \quad \text{(2)}$$

γ_o is crude oil gravity and PM_o is the molecular weight of the condensate. It is calculated from

$$\gamma_o = \frac{141.5}{131.5 + API} \quad \text{(3)}$$

$$PM_o = \frac{5954}{API - 8.81} \quad \text{(4)}$$

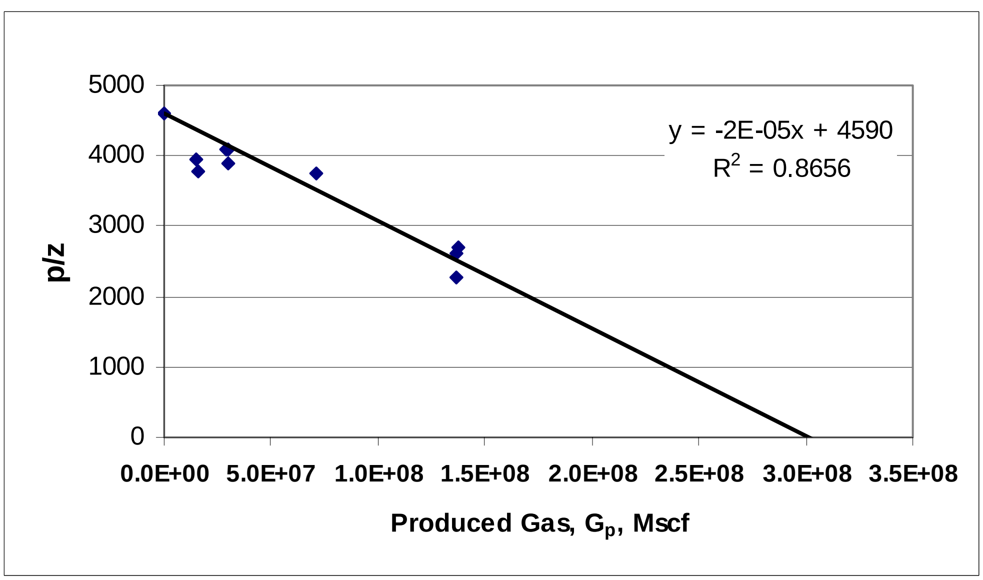

Fig. 2. 1 – Material balance plot for San Juan reservoir.

Fig. 2.1 includes information on 10 pressures and cumulative production values measured during the production history of the reservoir. The data are fit well by a straight line, indicating no pressure support from an aquifer. The original gas in place estimate is $3{,}1 \times 10^8$ Mscf (at p/z = 0). For an abandonment pressure of 10 percent of initial pressure (about 500 psia), the estimated ultimate recovery is 2.8×10^8 Mscf. As a comparison, the gas in place estimated from the volumetric method was 3.5×10^8 Mscf.

Given this initial material balance to establish the appropriate material balance model, we could proceed with our major objective: to find a method to quantify uncertainty in gas reserves estimates at any point in history and to find a method to update these reserves estimates.

To assess this uncertainty in reserve estimates, we used the methodology described below, which is based on Bayesian inversion methodology used to condition reservoir models to production data. The Bayesian inversion approach systematically combines prior knowledge and experience with a system to improve a prediction. In this way Bayesian inversion does not rely exclusively on the size of the data sample.

Bayesian inversion is one of the most widely used techniques in inversion problems[3]. It is based on a theorem from probability theory first proposed by the eighteenth-century English country clergyman and philosopher Thomas Bayes. To understand this theorem, let B_1, B_2, …, B_n, be n mutually exclusive and collectively exhaustive outcomes of some event B. Let A be an outcome of an "information event" or a "symptom" related to B. Note that A is not perfect information; it simply correlated to the event B. When A is perfect information about B, Bayes' theorem is not needed, but, in the more usual case, A is just a symptom that contains information useful in revising our prior probabilities about B. The revised probabilities are calculated using **Eq. 5**.

$$P(B_i / A) = \frac{P(A / B_i)P(B_i)}{\sum_{j=1}^{k} P(A / B_j)P(B_j)}, \quad i = 1,2,....k \text{ ……… ……………………} (5)$$

P(A / B_i) is the conditional probability that event A occurs when event B_i has occurred.

P(B_i) and *P(B_j)*, respectively, are the probabilities of events B_i and B_j

The result *P(B_i/A)* is also called the *probability of the causes* or *posteriori probability*. Bayes' theorem can be used in many applications in which we need to access the probabilities of the causes. For example, Bayesian inversion has achieved strong popularity in geophysical inversion problems.

Now, if we suppose that we know something about a model (e.g., from previous experience) before using available data. The prior knowledge and conjectures are called the *a priori* model. This knowledge is transformed into likelihoods or probabilities. Often likelihoods are assumed to follow a Gaussian distribution. Suppose we then have a set of data and also the statistical parameters describing the data (variance and covariance). The Bayesian approach provides a method to fine-tune the *a priori* model with the set of available data. The posterior distribution tells us how the data correct the prior knowledge.

In our case, Bayes' theorem becomes

$$P(G_i /(p / z)) = \frac{P((p / z) / G_i)P(G_i)}{\sum_{j=1}^{k} P((p / z) / G_j)P(G_j)}, \quad i = 1,2,.....k \text{ ……………………………} (6)$$

P(G_i) is the *a priori* distribution; *P* ((*p/z*)/G_i) is the likelihood of the model with parameters values *G*; *P (G_i)* and *P (G_j)* are the probabilities of events G_i and G_j; and *P*(G/*p/z*) is the conditional probability that the chosen G pertains to the real reservoir, given the misfit *(p/z)* calculated with an objective function used in regression analysis; and *P*(*p/z*) is the probability that a measurement has a value *p/z*.

We can rewrite **Eq. 6** as

$$P(G/(p/z)) = \left(P((p/z)/G) * P(G)\right) \quad \text{..... (7)}$$

From **Eq. 7**, we can calculate *P* (G/(p/z)), which is the *posteriori* probability distribution.

Lepine *et al.*[9], indicate that a suitable objective function for regression analysis, which represents how closely the calculated values from our modeling equation fit the observed data, and which includes both prior and *posteriori* terms is

$$F(G) = \frac{1}{2}\sum_{k=1}^{n} \frac{(p/z_k^{calc} - p/z_k^{obs})^2}{\sigma_l^{\,2}} + \frac{1}{2}\left(G^{calc} - G\right)^t C_G^{pri}\left(G^{calc} - G\right) \quad \text{..... (8)}$$

In **Eq. 8** G^{calc} is a randomly chosen gas in place, which must be between minimum and maximum values (three times the standard deviation). G is the most likely or average gas in place, and C^{pri} is the covariance matrix, which is the reciprocal of the Hessian matrix[8,9], which is the second derivative of objective function with respect the parameters in our model. σ_l is the standard deviation of measurement p/z^{Obsev}, and **t** indicates the transpose of a matrix. The values of the second term of the right hand of **Eq. 8** come from the volumetric estimate of gas in place in this application, and the values in the first term come from the available production data.

Now, consider the second term of the right hand of **Eq. 8**, which describes *prior* information:

$$-\frac{1}{2}\left((G^{Calc} - G)^t * C^{-1}(G^{Calc} - G)\right) \quad \text{..... (9)}$$

$(G^{Calc}-G)^t$ is the transpose of the matrix of errors. In our case because we have only one parameter, the matrix is an single number, and its transpose is the same number. In this specific case, C^{-1}, the inverse of the covariance matrix[8,9], is simply the reciprocal of the standard deviation of the prior information, σ_p, squared. Thus, **Eq. 9** can be written as

$$\frac{\sum_{i=1}^{nd}\left((G)^{Calc}-(G)^{Obs}\right)^2}{2\sigma_p^{\,2}} \quad \text{..... (10)}$$

The objective function then becomes

$$F(G)=\frac{\sum_{i=1}^{nd}\left(p/z^{calc}-p/z^{obs}\right)^2}{2\sigma_l^{\,2}}+\frac{\sum_{i=1}^{nd}\left(G^{calc}-G^{mean}\right)^2}{2\sigma_p^{\,2}} \quad \text{..... (11)}$$

where σ_l is the standard deviation of measurement data while σ_p is the standard deviation of the prior information (volumetric estimate of gas in place).

In **Eq. 11,** we can observe that the objective function takes in account prior and updated data. If we assume a Gaussian distribution, then[10]

$$P(G/(p/z)) \cong e^{-F(G)} \quad \text{..... (12)}$$

The maximum probability is reached when a minimum objective function is achieved. We reach this minimum when G^{calc} and p/z^{calc} are sufficiently close to the most likely values of G and p/z.

We can rewrite **Eq. 12** as

$$P(G/(p/z)) \cong e^{-\left(\frac{\sum_{i=1}^{nd}\left(p/z^{calc}-p/z^{obs}\right)^2}{2\sigma_l^{\,2}}\right)} * e^{-\left(\frac{\sum_{i-1}^{nd}\left(G^{calc}-G^{obs}\right)^2}{2\sigma_p^{\,2}}\right)} \quad \text{..... (13)}$$

The first term on the right hand of **Eq. 13** is the conditional probability that the second event occurs when first event has happened while the second term is the probability of first event. We know that the *prior* distribution, the first event, is described by the **Eq. 14**.

$$P(G) \cong e^{-\left(\frac{\sum_{i-1}^{nd}\left(G^{calc}-G^{obs}\right)^2}{2\sigma_p^{\,2}}\right)} \quad \text{..... (14)}$$

The average, G^{mean}, and the standard deviation, σ, define the probability density function of this parameter,

We now consider the probability density function of second event, which we call the likelihood function.

$$P((p/z)/G) \cong e^{-\left(\frac{\sum_{i=1}^{nd}\left((p/z)^{Calc}-(p/z)^{Obs}\right)^2}{2\sigma_l^{\,2}}\right)} \quad \text{..... (15)}$$

$(p/z)^{Obs}$ comes from field data and σ_l is the standard deviation of the misfit between $(p/z)^{Calc}$ and $(p/z)^{Obs}$.

From **Eq. 12**, we know that the must probable value of G, original gas in place, will be given by a maximum in P(G/(p/z)) or a minimum in f(G). It f (G) is minimized when the difference between calculated and observed data, is minimum.

Finally, we calculate the *posteriori* probability distribution, which is (Posteriori = Likelihood * Prior), as reflected in Eq. 7.

CHAPTER III
DISCUSSION AND RESULTS

In this chapter, we will apply the method described in Chapter II to the San Juan reservoir.

The posteriori probability density function is expressed by **Eq. 7**:

$$P(G/(p/z)) = \left(P((p/z)/G) * P(G)\right) \ldots\ldots\ldots\ldots\ldots\ldots\ldots\ldots\ldots\ldots\ldots\ldots \quad (7)$$

Unfortunately, for the San Juan reservoir, we know only the volumetric estimate of gas in place, G, and do not have sufficient information to determine the standard deviation associated with this estimate. Accordingly, we will assume a standard deviation and a normal distribution and check the sensitivity of our result to this assumption later. **Table 3.1** presents the known volumetric estimate and the assumed additional statistical information.

TABLE 3.1 – ASSUMED PRIOR STATISTICAL INFORMATION

	G,Mscf
mean, μ	3.50E+08
std, σ	1.06E+08
min	3.24E+07
max	6.68E+08
BIN	1.30E+07
n	50

We assumed a standard deviation, σ, of 1, 06 x 10^8 Mscf. "Min" is the minimum prior value expected, which we chose to be three standard deviations from the mean value. "Max" is the maximum prior value expected, which we again chose to be three standard deviations from the mean value. BIN is the interval we selected for each calculated

value. To build our prior probability density distribution, we assumed that 50 bins would be sufficient to span the range from minimum to maximum values of G.

We then calculated a probability distribution was calculated by application of Eq. 20. For example, for a G of 9.718×10^7 Mscf and data from (**TABLE 3.1)**, we calculated a probability of 2.17795×10^{-11}. This calculation was repeated for all 50 values of G. To normalize the probabilities, we divided each calculated value by the sum of the probabilities from all bins. For instance, dividing the probability of G being 9.718×10^7 Mscf, which is 2.17795×10^{-11} by the sum of all probabilities, 0.99876, we obtain the probability, 2.1803×10^{-11}, of this specific value occurring. Following this procedure, we generated the values displayed in **TABLE 3.2** and **Fig. 3.1.**

TABLE 3.2 – GAS IN PLACE AND ASSOCIATED PROBABILITY DISTRIBUTION

G,Mscf	P(G)	G,Mscf	P(G)	G,Mscf	P(G)
3.24E+07	0.01	2.53E+08	0.59	4.73E+08	0.46
4.53E+07	0.01	2.66E+08	0.66	4.86E+08	0.39
5.83E+07	0.02	2.79E+08	0.72	4.99E+08	0.33
7.12E+07	0.03	2.92E+08	0.77	5.12E+08	0.28
8.42E+07	0.04	3.05E+08	0.82	5.25E+08	0.23
9.72E+07	0.05	3.18E+08	0.86	5.38E+08	0.19
1.10E+08	0.07	3.31E+08	0.89	5.51E+08	0.15
1.23E+08	0.09	3.44E+08	0.90	5.64E+08	0.12
1.36E+08	0.12	3.56E+08	0.90	5.77E+08	0.09
1.49E+08	0.15	3.69E+08	0.89	5.90E+08	0.07
1.62E+08	0.19	3.82E+08	0.86	6.03E+08	0.05
1.75E+08	0.23	3.95E+08	0.82	6.16E+08	0.04
1.88E+08	0.28	4.08E+08	0.77	6.29E+08	0.03
2.01E+08	0.33	4.21E+08	0.72	6.42E+08	0.02
2.14E+08	0.39	4.34E+08	0.66	6.55E+08	0.01
2.27E+08	0.46	4.47E+08	0.59	6.68E+08	0.01
2.40E+08	0.52	4.60E+08	0.52		

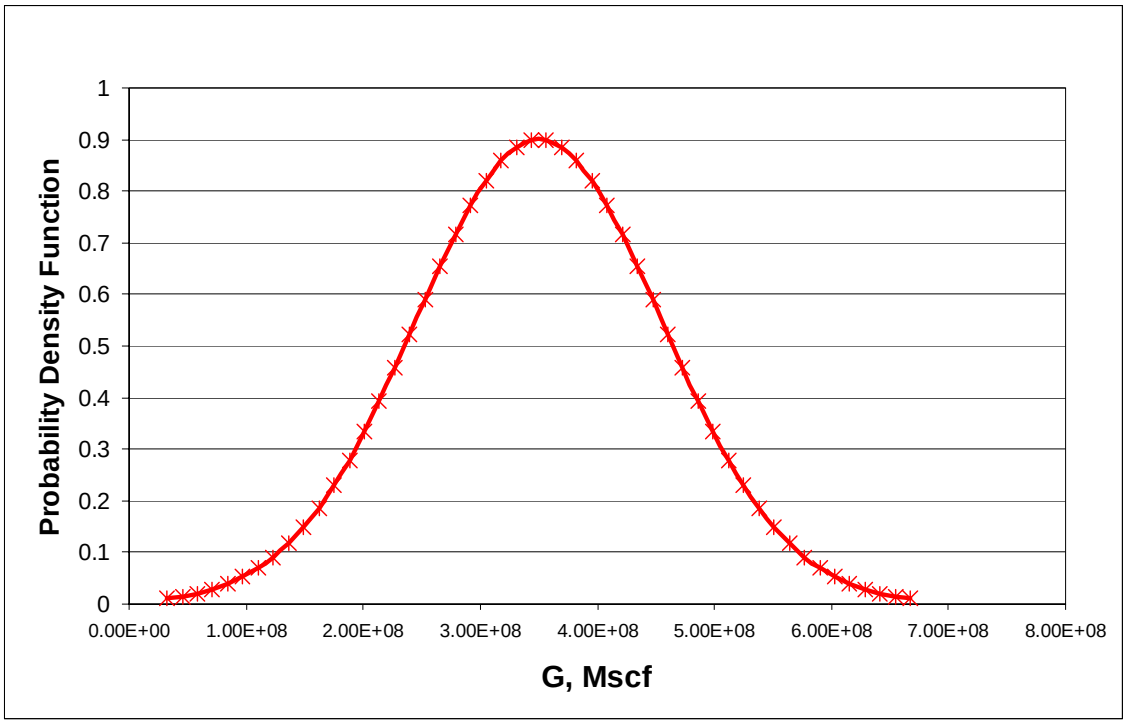

Fig. 3. 1 – Assumed probability density function for gas in place.

Next, we estimated a likelihood probability distribution function, using the available production data. First, to obtain $(p/z)^{Calc}$, we used the material balance equation, **Eq. 16.**

$$\frac{P}{Z} = \frac{P_i}{Z_i}\left[1 - \frac{G_P}{G}\right] \qquad (16)$$

G_p is the cumulative gas production that from field data (**TABLE 2.1**), and G values are the same as the values chosen for the Prior probability distribution. This calculation is done for each new available pressure and the corresponding cumulative gas produced.

$(p/z)^{Obsev}$ comes from field data (**TABLE 2.1**), and σ_l is the standard deviation of the measurements p/z^{Obsev}.

In this way, we calculated p/z for the full range of G values (minimum to maximum) for each G_p value reported at measurement points. This allowed us to then calculate the likelihood density distribution (which is, again, normalized so that the sum of the likelihoods is exactly unity). The likelihood density distribution required 500 calculations (10 values of G_p and 50 values of G). We developed a subroutine in Visual Basic to perform these calculations. The results are given in **Table 3.3** and **Fig. 3.2**.

This likelihood represents the probability of each *prior* value for the observed cumulative production of gas.

TABLE 3.3 – LIKELIHOOD PROBABILITY DENSITY DISTRIBUTION

G,Mscf	P((p/z)/G)	G,Mscf	P((p/z)/G)	G,Mscf	P((p/z)/G)
3.24E+07	0.00	2.53E+08	0.34	4.73E+08	0.10
4.53E+07	0.00	2.66E+08	0.43	4.86E+08	0.09
5.83E+07	0.00	2.79E+08	0.50	4.99E+08	0.08
7.12E+07	0.00	2.92E+08	0.54	5.12E+08	0.06
8.42E+07	0.00	3.05E+08	0.55	5.25E+08	0.06
9.72E+07	0.00	3.18E+08	0.53	5.38E+08	0.05
1.10E+08	0.00	3.31E+08	0.50	5.51E+08	0.04
1.23E+08	0.00	3.44E+08	0.45	5.64E+08	0.04
1.36E+08	0.00	3.56E+08	0.41	5.77E+08	0.03
1.49E+08	0.00	3.69E+08	0.36	5.90E+08	0.03
1.62E+08	0.00	3.82E+08	0.31	6.03E+08	0.02
1.75E+08	0.00	3.95E+08	0.27	6.16E+08	0.02
1.88E+08	0.01	4.08E+08	0.23	6.29E+08	0.02
2.01E+08	0.02	4.21E+08	0.20	6.42E+08	0.02
2.14E+08	0.06	4.34E+08	0.17	6.55E+08	0.01
2.27E+08	0.14	4.47E+08	0.14	6.68E+08	0.01
2.40E+08	0.23	4.60E+08	0.12		

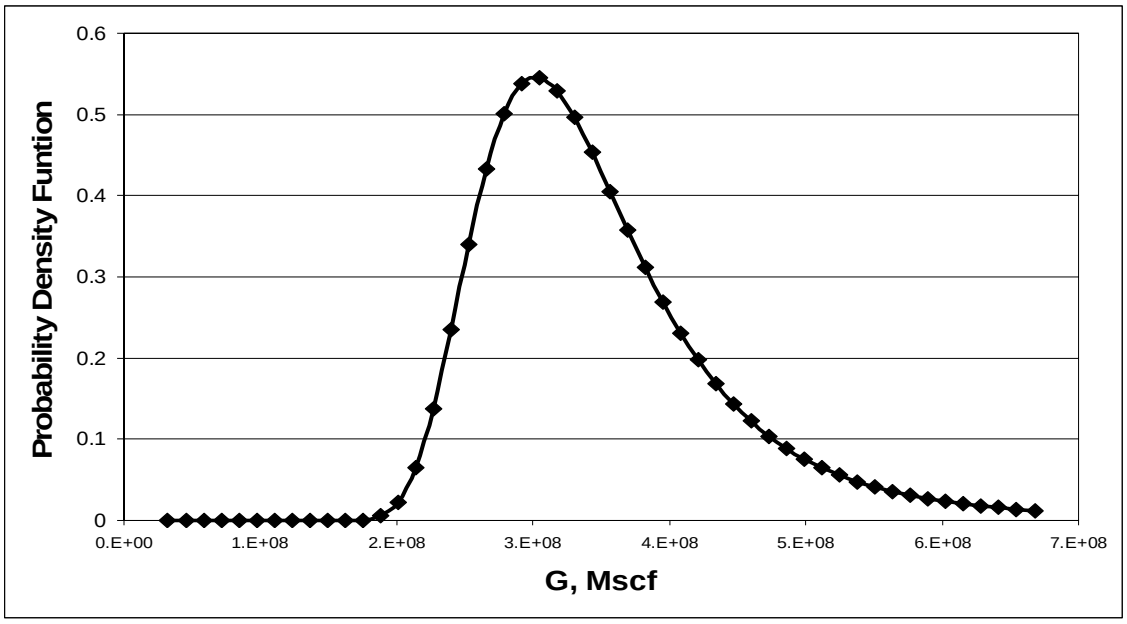

Fig. 3. 2 – Likelihood probability density function.

Finally, we calculated the *posteriori* probability distribution, which, schematically, is

Posteriori = Likelihood * Prior

It is instructive at this point to examine the traditional p/z vs. G_p ance plot. (**Fig. 3.3)**, in which, we can see the integration between prior information and the updated information (the likelihood function).

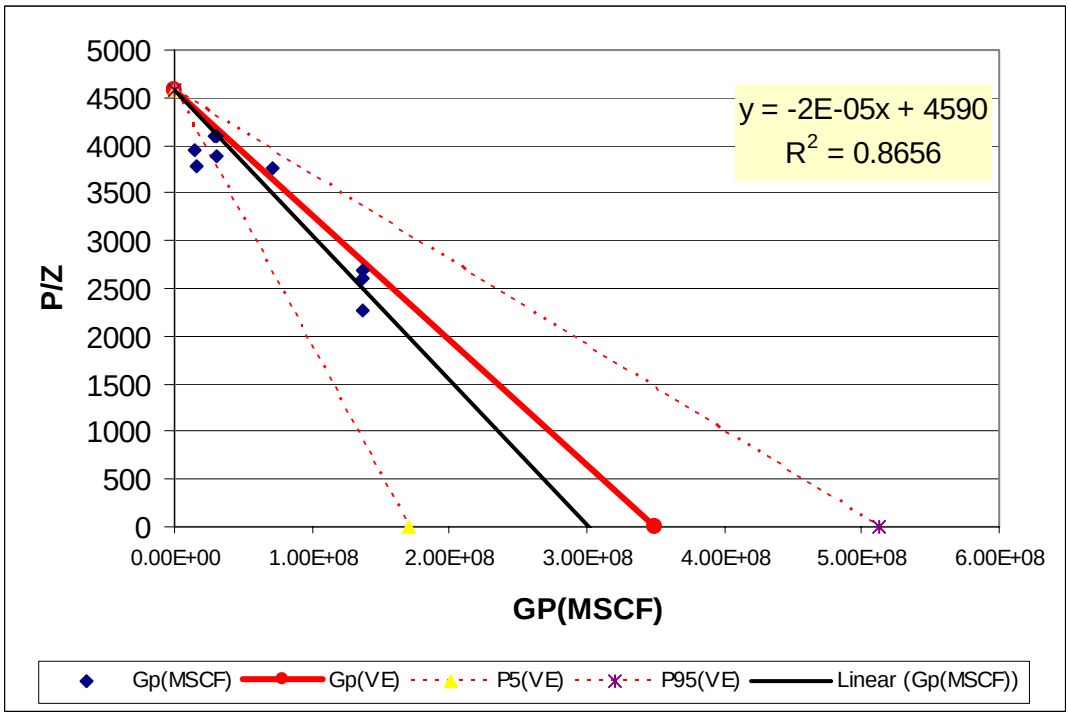

Fig. 3. 3 – Material balance (p/z) plot for San Juan reservoir.

This plot shows an area bounded by dashed red lines, which represent the P_5 and P_{95} limits of uncertainty for the volumetric estimate of gas in place, G. The area between these limits represents the uncertainty range of any p/z vs. G_p for this reservoir (prior information) while the solid red line represents the prior average value. The black line represents the p/z vs. G_p regression with available information (likelihood).

The next step in our calculations is to multiply likelihood probability density function by the prior density probability function. The results are given in **Table 3.4** and **Fig. 3.4.**

TABLE 3.4 – *POSTERIORI* PROBABILITY DENSITY DISTRIBUTION

G,Mscf	P(G/(p/z))	G,Mscf	P(G/(p/z))	G,Mscf	P(G/(p/z))
3.24E+07	0.00	2.53E+08	0.20	4.73E+08	0.05
4.53E+07	0.00	2.66E+08	0.28	4.86E+08	0.03
5.83E+07	0.00	2.79E+08	0.36	4.99E+08	0.03
7.12E+07	0.00	2.92E+08	0.42	5.12E+08	0.02
8.42E+07	0.00	3.05E+08	0.45	5.25E+08	0.01
9.72E+07	0.00	3.18E+08	0.45	5.38E+08	0.01
1.10E+08	0.00	3.31E+08	0.44	5.51E+08	0.01
1.23E+08	0.00	3.44E+08	0.41	5.64E+08	0.00
1.36E+08	0.00	3.56E+08	0.36	5.77E+08	0.00
1.49E+08	0.00	3.69E+08	0.32	5.90E+08	0.00
1.62E+08	0.00	3.82E+08	0.27	6.03E+08	0.00
1.75E+08	0.00	3.95E+08	0.22	6.16E+08	0.00
1.88E+08	0.00	4.08E+08	0.18	6.29E+08	0.00
2.01E+08	0.01	4.21E+08	0.14	6.42E+08	0.00
2.14E+08	0.03	4.34E+08	0.11	6.55E+08	0.00
2.27E+08	0.06	4.47E+08	0.08	6.68E+08	0.00
2.40E+08	0.12	4.60E+08	0.06		

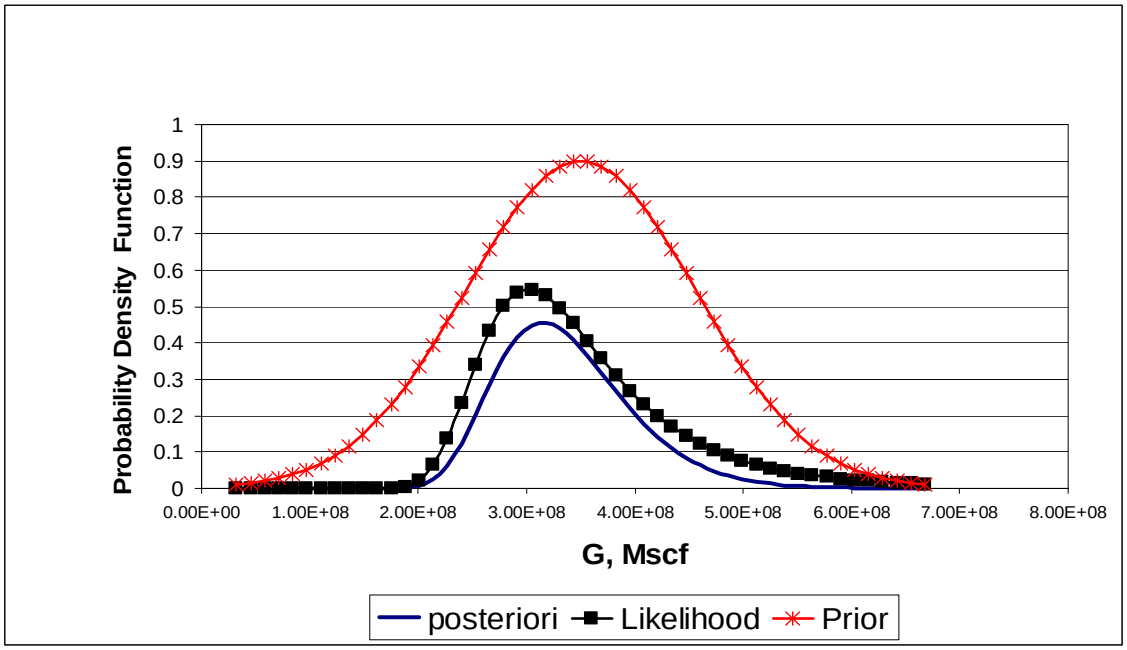

Fig. 3. 4 – Probability density function for prior, likelihood and posterior distributions**.**

In addition to developing methodology to assess uncertainty using prior knowledge with updated data, we also developed a method to determine how the range of uncertainty in reserve estimates changed with time in the history of the San Juan reservoir.

To estimate the change of range of uncertainty in reserves (or gas in place initially) starting in the initial stages of development of San Juan Reservoir, we first defined the range of uncertainty to be 90 percent; i.e., from P_5 (minimum) to P_{95} (maximum). We determined this range from the cumulative density function for prior information (**Fig. 3.5**)

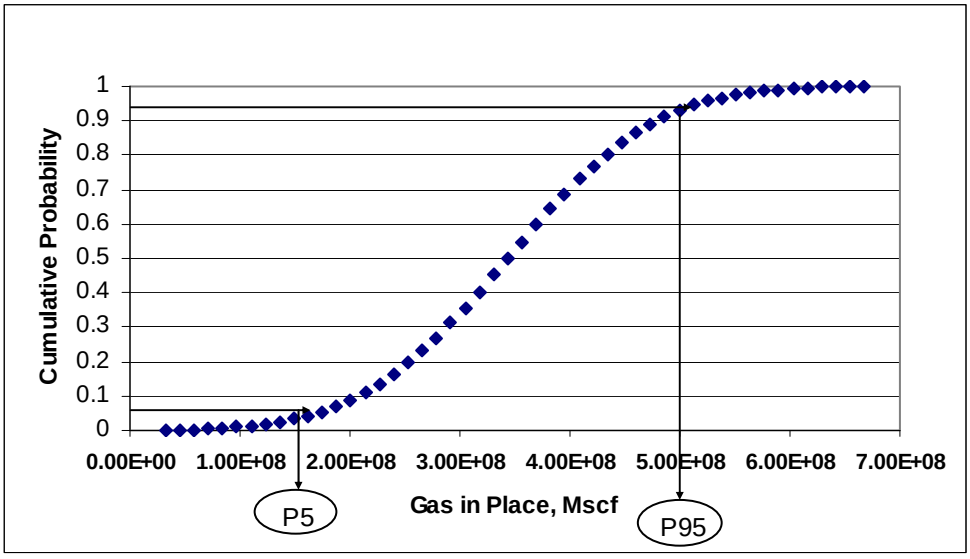

Fig. 3. 5 – Cumulative density distribution for prior information.

Next, we subdivided the production history data into four ranges: Very-Early, Early, Middle and Late, which are identified in **TABLE 3.5.**

TABLE 3.5 – SEGMENTED HISTORY RANGES

Stage	Date	P/z	G_p, Mscf
Very-Early	15/12/72	4590	0.00E+00
	31/08/81	3941	1.51E+07
Early	1/4/1982	3787	1.62E+07
	1/11/1984	4095	2.89E+07
	30/11/84	4099	3.00E+07
	30/11/84	3897	3.00E+07
Middle	30/09/89	3759	7.11E+07
Late	13/02/01	2609	1.37E+08
	16/02/01	2267	1.37E+08
	10/4/2001	2693	1.37E+08

Briefly, using the same *a priori* distribution that we presented in Table 3.2 and Fig. 3.3, we updated the reserve estimation from the "Very Early Time" period through the "Late Time" period, using the additional data available in each period. We found that the range of uncertainty (the difference between P_{95} and P_5) decreased as more data was added to the likelihood model. (**TABLE 3.6** and **Fig. 3.5**). Note that Estimated Ultimate Recovery (EUR) is cumulative gas production expected at an abandonment pressure of 10 percent of the discovery pressure in the San Juan reservoir and is thus roughly 90 percent of the original gas in place.

TABLE 3.6 – UNCERTAINTY RANGES IN DIFFERENT TIME PERIODS

Estimated Ultimate Recovery , Mscf				
Period	Average	P_{95}	P_5	Volumetric estimate
Prior	3.15E+08	4.66E+08	1.49E+08	3.15E+08
Very-Early	2.97E+08	4.61E+08	1.44E+08	3.15E+08
Early	2.04E+08	3.54E+08	1.53E+08	3.15E+08
Middle	2.74E+08	3.83E+08	2.10E+08	3.15E+08
Late	2.86E+08	3.93E+08	2.22E+08	3.15E+08

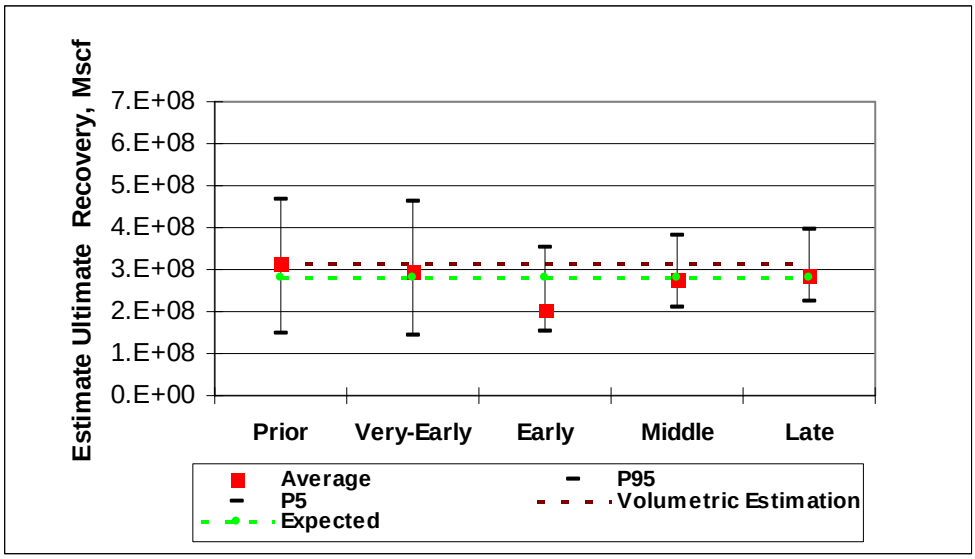

Fig. 3. 6– Graphical display of varying ranges of uncertainty in EUR estimates with time.

In Fig. 3.6, the vertical axis is the EUR and the horizontal axis is the time period in reservoir history. "Prior" represents the reserve estimate based on volumetric calculations, which is usually the first reserve estimate available.

"Very-Early" represents the first period of reservoir life, in which we used limited production data to update the range of uncertainty. There was little change in the range, partly because the data were very poor and partly because of the limited amount of data. In the next period ("Early) in which more data was added, a clear decrease in the range of uncertainty was obtained, and the most likely estimate is closer to the final expected value.

We next performed a sensitivity study to determine the effect of altered values of volumetric estimates of original gas in place. We studied two sensitivities, with G increased and decreased by 33 percent from the value actually reported to us. The results are shown in **Tables 3.7** and **3.8** and **Figures 3.7** and **3.8.** From these this sensitivity study, we conclude that, even when the most likely prior estimate is

moderately incorrect, the most likely or “true” value lies within the estimated range of uncertainty. Additionally, as more data are added, the more weight the likelihood model (based on actual production performance) has.

TABLE 3.7 – VOLUMETRIC EUR DECREASED BY 33 % OF MOST LIKELY VALUE

Estimated Ultimate Recovery , Mscf				
Period	Average	P_{95}	P_5	Volumetric estimate
Prior	2.10E+08	3.51E+08	5.22E+07	2.10E+08
Very-Early	1.81E+08	3.69E+08	8.70E+07	2.10E+08
Early	1.81E+08	2.99E+08	1.50E+08	2.10E+08
Middle	2.50E+08	3.55E+08	1.98E+08	2.10E+08
Late	2.62E+08	3.51E+08	2.04E+08	2.10E+08

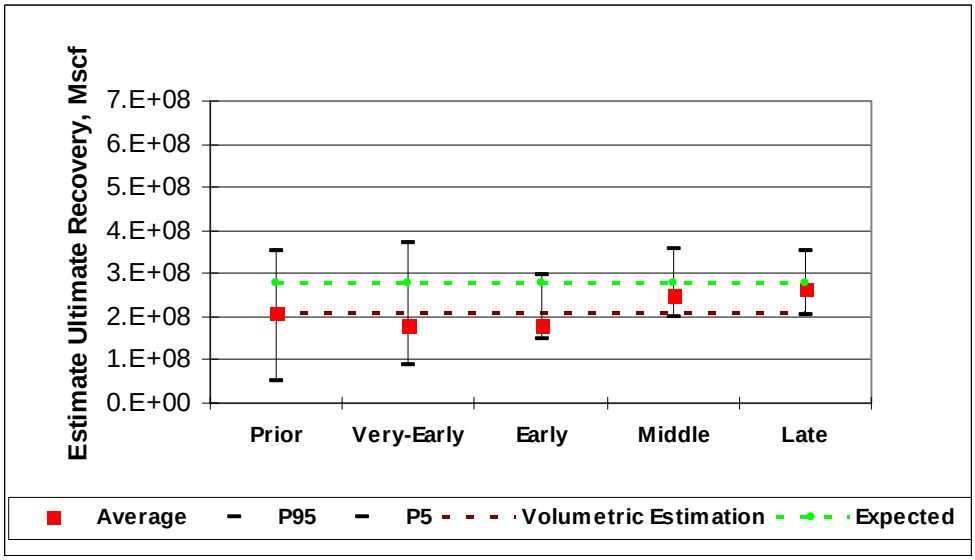

Fig. 3. 7– Time variation of uncertainty, decreased volumetric estimate.

TABLE 3.8 –VOLUMETRIC EUR INCREASED BY 33 % OF MOST LIKELY VALUE

Estimated Ultimate Recovery , Mscf				
Period	Average	P_{95}	P_5	Volumetric estimate
Prior	4.14E+08	5.71E+08	2.50E+08	4.14E+08
Very-Early	4.09E+08	5.57E+08	2.42E+08	4.14E+08
Early	2.85E+08	4.45E+08	1.71E+08	4.14E+08
Middle	3.37E+08	4.47E+08	2.27E+08	4.14E+08
Late	3.63E+08	4.57E+08	2.40E+08	4.14E+08

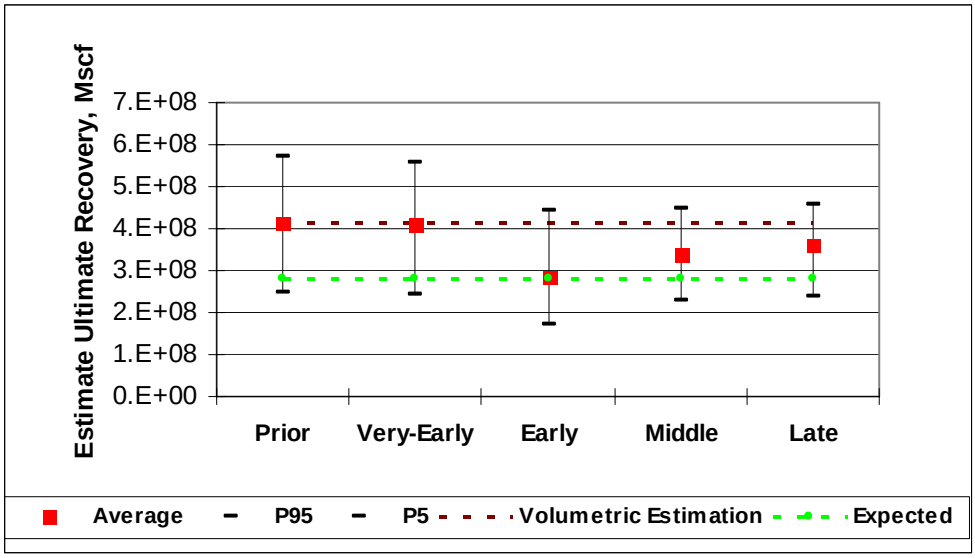

Fig. 3. 8 – Time variation of uncertainty, volumetric estimate increased.

We examined two additional sensitivities, in which we first doubled and then halved the assumed the standard deviation of the volumetric estimate probability distribution. The results are given in **Tables 3.9** and **3.10** and in **Figs. 3. 9 and 3.10**. From these two sensitivity studies, we conclude that, if *a priori* information has a large range of uncertainty, the range is narrowed as new production data become available. Also we can conclude that with both "large" and "small" standard deviations, the most likely or "true" value lies within the range of uncertainty estimated.

TABLE 3.9 – STANDARD DEVIATION IN VOLUMETRIC EUR DOUBLED

Estimated Ultimate Recovery , Mscf				
Period	Average	P_{95}	P_5	Volumetric estimate
Prior	3.15E+08	6.16E+08	0.00E+00	3.15E+08
Very-Early	2.33E+08	5.04E+08	7.97E+07	3.15E+08
Early	1.87E+08	3.24E+08	1.26E+08	3.15E+08
Middle	2.57E+08	3.88E+08	1.95E+08	3.15E+08
Late	2.80E+08	4.05E+08	2.07E+08	3.15E+08

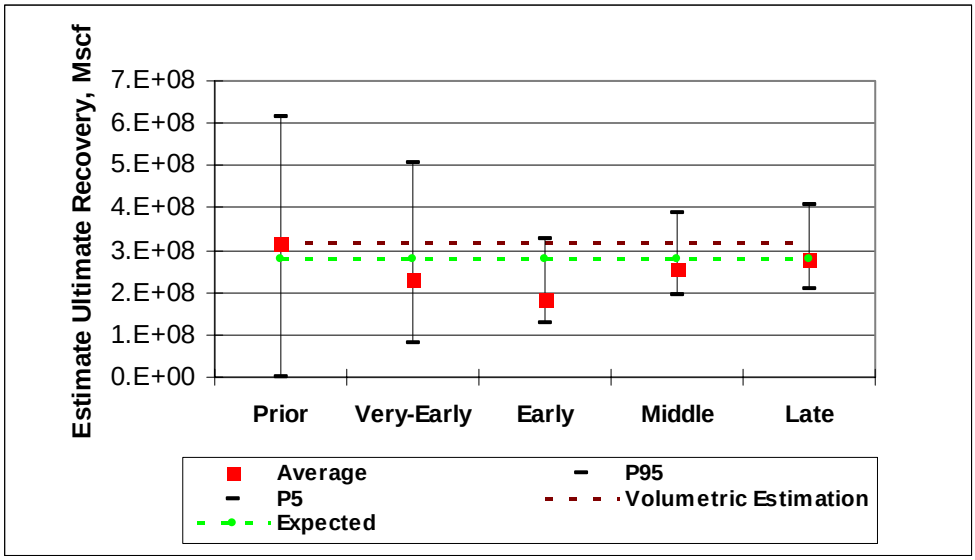

Fig. 3. 9 – Time variation of uncertainty, standard deviation in volumetric estimate doubled.

TABLE 3.10 – STANDARD DEVIATION IN VOLUMETRIC EUR HALVED

Estimated Ultimate Recovery , Mscf				
Period	Average	P_{95}	P_5	Volumetric estimate
Prior	3.15E+08	3.92E+08	2.36E+08	3.15E+08
Very-Early	3.12E+08	3.88E+08	2.30E+08	3.15E+08
Early	2.77E+08	3.53E+08	2.05E+08	3.15E+08
Middle	2.95E+08	3.65E+08	2.34E+08	3.15E+08
Late	3.00E+08	3.71E+08	2.41E+08	3.15E+08

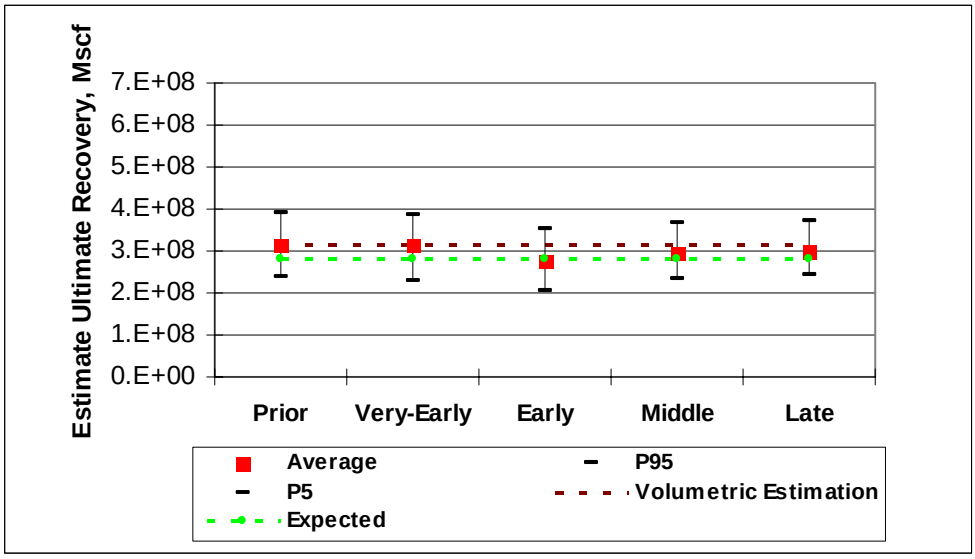

Fig. 3. 10 – Time variation of uncertainty, standard deviation in volumetric estimate halved.

CHAPTER IV
SUMMARY AND CONCLUSIONS

Our study of the ranges of uncertainties in San Juan Reservoir, Santa Rosa Field, led us to draw certain conclusions. First, the methodology we have discussed appears to be generally useful to quantify uncertainty in reserve estimates, combining previous knowledge with updating data when dealing with limited data. Further, with prior knowledge and updated data, we calculate different likelihoods for reserves in each stage of the reservoir life and different, but reliable, ranges of uncertainty (Figs. 3.5 and 3.7).

We also conclude that the estimation of *posteriori* likelihood values for each model based on prior probabilities and available production data can lead to good estimates of uncertainty for a given model; therefore, having complete and accurate geological knowledge for the *a priori* model could lead to very narrow ranges and realistic estimations of uncertainties and outcomes.

For the San Juan Reservoir, the OGIP was estimated to be in the range 2.8 - 3.12 x 10^8 Mscf which agrees well with previous estimates.

We also conclude that the validation and evaluation of observed data is an important, and fundamental, part of any history matching process because this process gives us insight into the uncertainty of the measurements, the relative importance of the observations with time and also relative to each other. The goodness of fit of a history match simulation is judged against this observed data and its uncertainties.

Finally, we believe that this method could be extended to more general material balance methods, such as those proposed by Havlena and Odeh[11], in which the material balance is expressed as the equation of straight line. Material balance equations with more than one unknown (e.g., both original oil in place and gas cap volume) should be adaptable to extensions of our basic method.

NOMENCLATURE

Variables

C	=	covariance
Calc	=	calculated
EUR	=	estimated ultimate recovery, scf
G	=	gas in place, scf
GE	=	gas equivalent, scf/stb
G_P	=	produced gas, scf
G_{PT}	=	produced gas plus gas equivalent, scf
K	=	permeability
N_P	=	produced oil, stb
Obs	=	observed
OGIP	=	original gas in place, scf
p	=	pressure, psia
PM_0	=	condensate gas molecular weight
P()	=	probability
S	=	saturation
W_i	=	weight factor for data point i.
$y_{calc,i}$	=	calculated value at point i
$y_{obs,i}$	=	observed data point i
z	=	gas deviation factor
γ_O	=	crude oil gravity
σ	=	standard deviation
ϕ	=	reservoir porosity, fraction
μ	=	viscosity, cp

Subscripts

g	=	gas
i	=	measurement data

j = variables

l = likelihood of measurement data

o = oil

p = prior

r = relative

w = water

REFERENCES

1. Floris, F. J., Bush, M. D., Cuypers, M., Roggero, F. and Syversveen, A. R: "Methods for Quantifying the Uncertainty of Production Forecasts: A Comparative Study," *Petroleum Geosciences* (2001) **7**, 87-97.
2. McVay, D.A. and Lee, W. J.*:* "Calibration Improves Uncertainty Quantification through the Reservoir Life Cycle: paper OTC, Offshore Technology Conference, 48997, presented at the Offshore Technology Conference and Exhibition held in Houston, Texas 5-8 May 2003.
3. Department of Petroleum Texas A&M paper (2003).
4. Nepveu, M.: "Hydrocarbon Production Forecasting with Limited Data – How to Fill the Gaps," *Proc*., 7th European Conference on the Mathematics of Oil Recovery, Baveno, Italy (2000) V-5.
5. Egberts, P.J.P., Brouwer, G.K. and Bos, C.F.M.: "History Matching and Forecasting with Uncertainty Quantification: A Real Case Study," paper presented at the 2002 EAGE European Association of Geoscientists and Engineers, Florence, Italy, 27th May.
6. "San Juan Reservoir, Santa Rosa Field Overview," Internal report PDVSA, Petróleo de Venezuela Sociedad Anónima, Caracas (October 2001).
7. "Initial Evaluation of the Study of Simulation Merecure, Unit II-Cycle 4 and in the Cretaceous, San Juan A/B. Field Santa Rosa". LIC Santa Rosa. INT-8160, 2000. Technical Report PDVSA, Caracas (October 2001).
8. "Static Model Formation Merecure, Vidoño, San Juan and San Antonio, Field Santa Rosa, LIC Santa Rosa". INT-7531, 2000. Technical Report. PDVSA, Caracas (October 2000).

9. Floris, F.J.T. and Peersmann, M.R.: "Uncertainty Estimation in Volumetric for Supporting Hydrocarbon Exploration and Production Decision Making," *Petroleum Geosciences* (1998) **4**, 33-40

10. Lepine, O. J., Bissell R. C., Aanonsen, S. I., Pallister, I. and Barker, J. W. "Uncertainty Analysis in Predictive Reservoir Simulation Using Gradient Information," paper SPE 48997, presented at the SPE Annual Technical Conference and Exhibition held in New Orléans, Louisiana 27-30 September 1998.

11. Bronshtein I. and Semendyayev K. (ed) *Handbook of Mathematics*, 3rd edition, Springer-Verlag, New York (1998), 598-635.

12. Havlena, D. and Odeh, A.S.:"The Material Balance Equation as an Equation of a Staraight Line," *JPT* (Aug. 1963) **2**, 896-900 *Trans*., AIME, **228.**

13. *SimOpt User's Guide*, Schlumberger, Houston, TX (2002).

APPENDIX

History Matching with Reservoir Simulator

Single Cell Model

After establishing with material balance calculations that the San Juan reservoir is volumetric (no influx of water from an aquifer), we built a single-cell model to refine the material balance results. We obtained data for this model from PDVSA. We used the following data in this model:

Average Net pay:	253 ft.
Average Net thickness:	1500 ft.
Average Porosity:	8.5 %
Permeability:	40 md
X grid block size:	9500 ft.
Y grid block size:	7500 ft.
Depth of top face:	9600 ft.

Production Data

Extensive production data was collected from the current field operator, PDVSA. The production reports contained monthly cumulative oil, water and gas production for each individual well that was drilled and put on production since the field was discovered in 1973. After 28 years of production, the vast amount of data from eight producers was manipulated until it was suitable for incorporation into the reservoir model as a single well. A single historical data file containing the cumulative monthly production of all the wells was built in a form of a rate schedule for production. Thus, the primary operational constraint is the gas rate and the secondary constraint is the flowing bottom-hole pressure.

Reservoir Fluid Properties

Reservoir fluid studies were conducted on samples taken from the wells RG173 and RG190. Even though this reservoir has been classified as condensate reservoir, for purpose of this research it will be treated as a wet gas reservoir mostly because so little condensate forms in the reservoir. The phase diagram for reservoir fluid, **Fig. A.1**, shows that the maximum amount of liquid formed is less than 2% of the reservoir volume. Additionally, the producing gas-oil ratio is more than 32,000 scf/STB, confirming that we can treat the reservoir as containing wet gas.

Fluid properties for the well RG190 were determined to be more representative than those from well RG173. The dew point was 4,014 psig, and at this pressure the gas viscosity is 0.0255 cp. The gravity of the oil is 43° API and the formation volume factor is about 7 RB/STB. For this simulation, the PVT table was built from standard oil and gas correlations based on a liquid with gravity 43° API, gas density 0.0641 lb/ft^3 at discovery pressure, reservoir temperature 260°F, dew-point pressure 4,014 psig and a maximum reservoir pressure of 4,600 psig (**Fig. A-2)**. Similarly, the reservoir water properties are estimated from correlations based on a water density 62 lbs/ft^3, water compressibility 9.7E-6 1/psi, and water viscosity 0.45 cp.

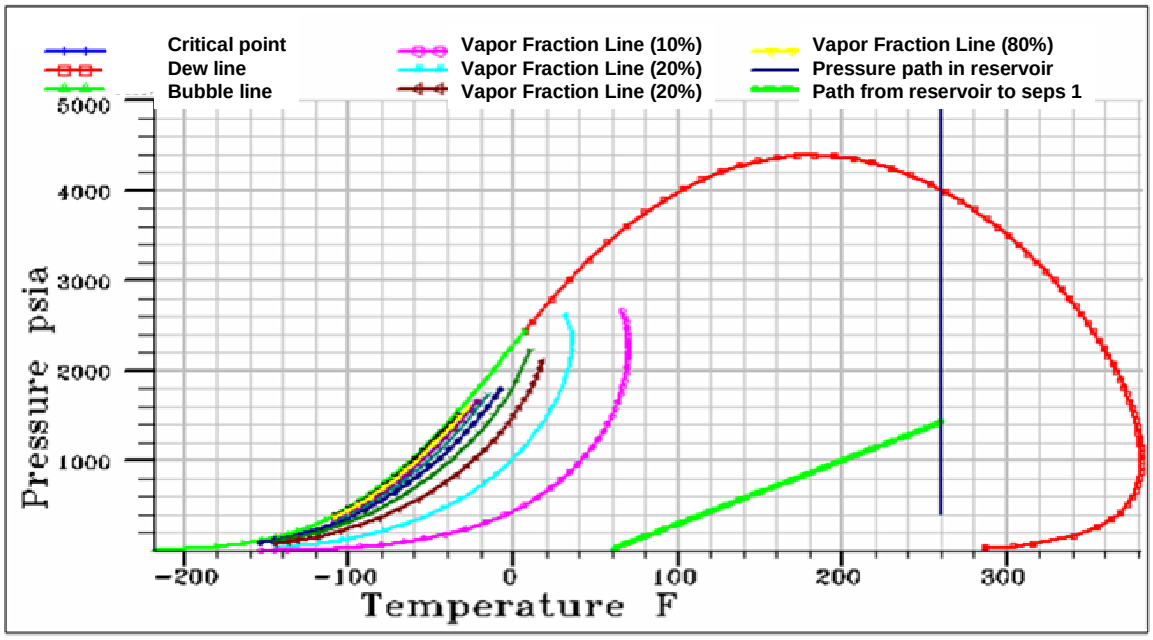

Fig. A.1 – Phase diagram, San Juan Reservoir gas.

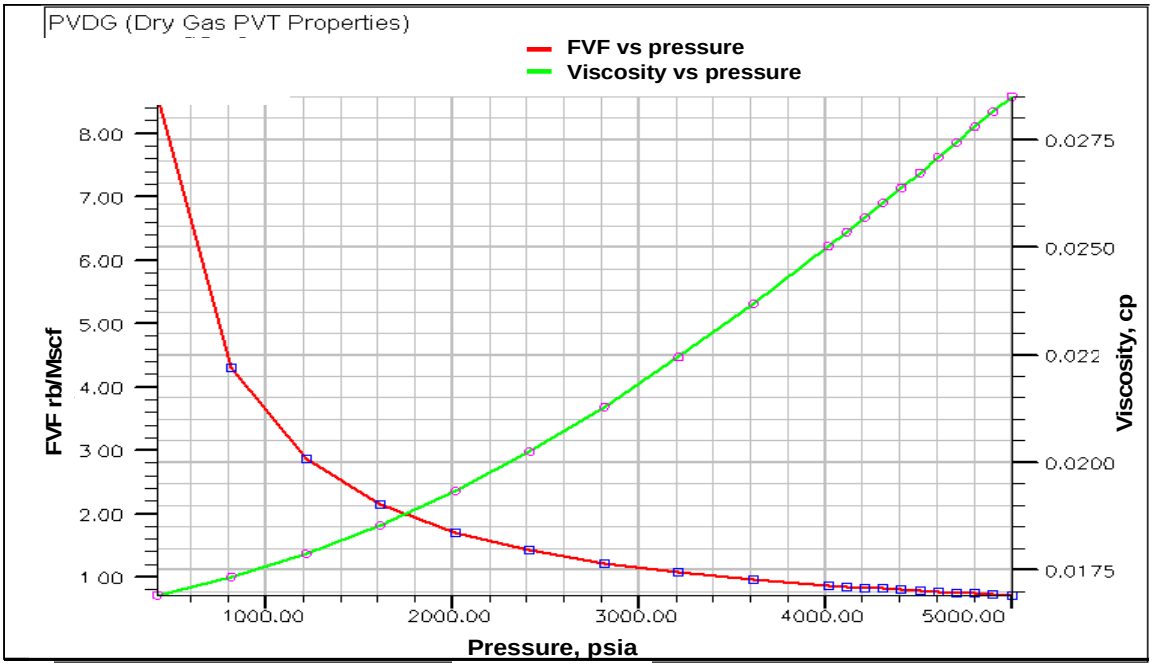

Fig. A.2 – Formation volume factor and viscosity, San Juan Reservoir gas.

Relative Permeability

The initial set of relative permeability curves incorporated in the reservoir model corresponds to well RG231 core analysis. The water-oil and gas-oil relative permeability curves reported for the well were based on the correlation of Honarpour, using a connate water saturation of 0.1, residual oil saturation to water of 0.19 and average permeability of 40 md. The initial saturation-dependent relative permeability properties for oil water and gas are shown in Table **A. 1** and graphically in **Fig. A. 3.** These relative permeability data were not adjusted in this study because we ultimately modeled only single-phase gas flow.

TABLE A.1 – GAS–WATER RELATIVE PERMEABILITY FUNCTIONS.

S_w	K_{rw}	K_{rg}
0.1	0	1
0.19	0.000617	0.702332
0.28	0.004938	0.470508
0.37	0.016667	0.296296
0.46	0.039506	0.171468
0.55	0.07716	0.087791
0.64	0.133333	0.037037
0.73	0.211728	0.010974
0.82	0.316049	0.001372
0.91	0.45	0
1	1	0

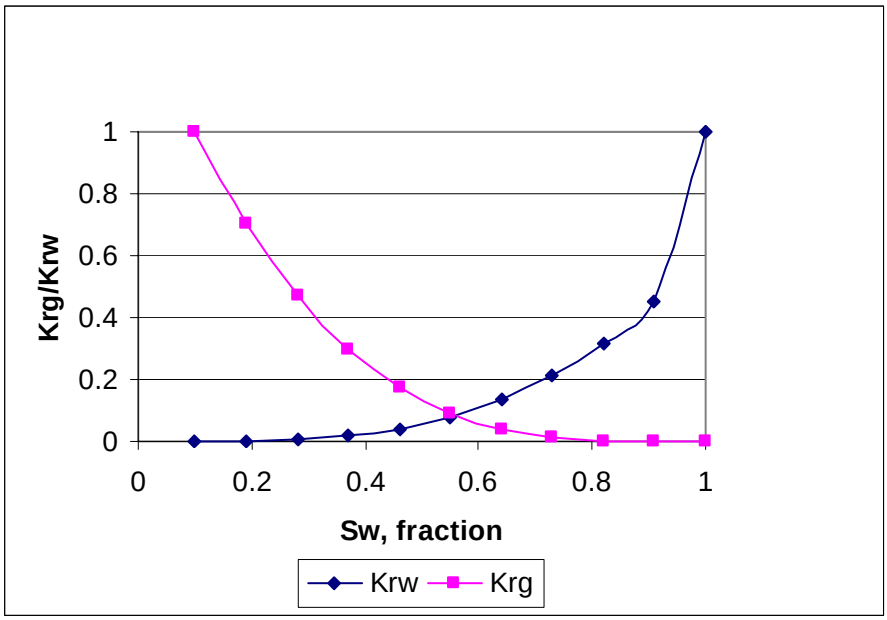

Fig. A.3 – Gas-water relative permeability functions, San Juan Reservoir.

Pressure Data

The analysis of pressures in San Juan Reservoir was to take to a same datum the pressures available in cretaceous' sands, SJ-UA, SJ-UB, and SJ-UC, since these are the some measures of pressure in wells pertaining to San Juan Reservoir **(TABLE A. 2)** and **(Fig. A.4)**. the analysis of pressures includes the analysis of communication between these formation and determination of value of the datum that better represents the behavior of declination of pressure in that reservoir.

TABLE A.2 – AVERAGE BLOCK PRESSURE- SAN JUAN RESERVOIR

Date	Well	Middle point	Grad well (psia/Ft)	Perf depth(Ft)	P @ 9600* (psia)	P @ 9788* (psia)	P@ 10000* (psia)	P @ 10200* (psia)	P @ 10500* (psia)
15/12/72	RG 134	4365	0.11	10319					4679
31/08/81	RG 173	3725	0.07	10810	3716	3731	3748	3764	3788
1/4/1982	RG 134	3303	0.11	10364	3298	3359	3435	3503	3606
1/11/1984	RG 134	3676	0.11	10364	3671	3732	3808	3876	3979
30/11/84	RG 200	3662	0.09	10367	3675	3736	3812	3881	3984
30/11/84	RG 200	3497	0.05	10570	3424	3486	3563	3632	3736
30/09/89	RG 173	3451	0.34	10375	3473	3493	3518	3541	3575
13/02/01	RG 216	2097	0.06	10367	2088	2149	2225	2293	2396
16/02/01	RG 188	1781	0.06	10367	1770	1831	1907	1976	2079
10/4/2001	RG 190	2175	0.06	10367	2168	2229	2305	2374	2476

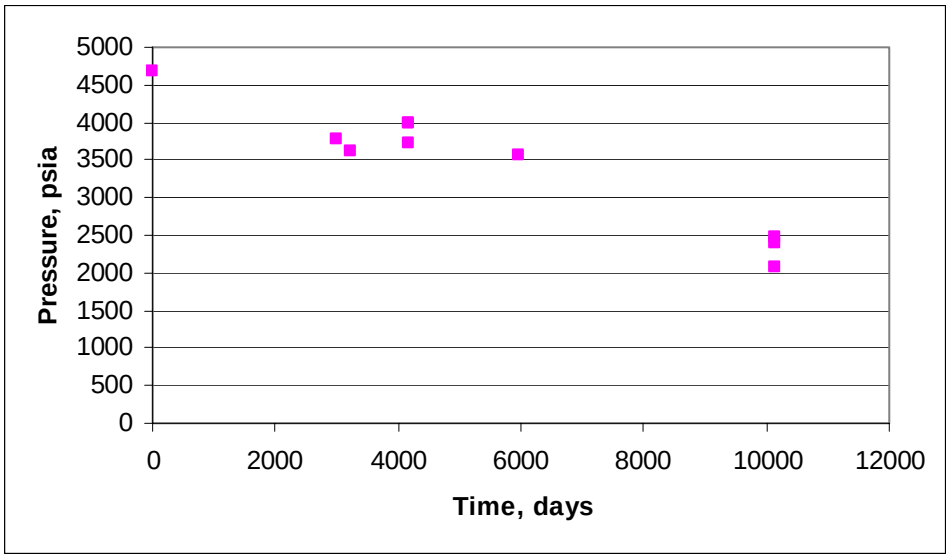

Fig. A.4 – Average static bottom-hole pressure at individual wells.

The bottom-hole pressure measured in individual wells were corrected to a common mid-perforation elevation and then plotted all together against time. Because some wells

are located in different regions of the reservoir, and however they are measuring a very similar bottom hole pressure. Therefore, it is interpreted that the bottom-hole pressure measured at static conditions in some of the producing wells may be representative of the average reservoir pressure. The pressure data points showed in (**Fig. A. 4**) is the result of an arithmetic mean for the average reservoir pressure, which was calculated to be on the middle point of reservoir.

History Match Single-Cell Model

The observed data available consisted of static bottom-hole pressures and water, oil and gas rates from 1973 to 2001. We used the SIMOPT[5] module of Eclipse to history match the observed data (essentially, only pressures).

The purpose of a history match is to minimize the difference between observed and simulated values. This difference is reflected in an objective function whose decrease in value is a measure of an improving match. The observed data objective function in SIMOPT is the weighted sum of the squares of the mismatch divided by the measurement error, which is expressed as

$$\sum_i \left\{ w_i \times \left(\frac{y_{obs,i} - y_{Calc,i}}{\sigma} \right) \right\}^2 \quad \text{.....} \quad (17)$$

where W_i is weight factor for data point I, $y_{obs,i}$ is observed data point I, $y_{calc,i}$ is the calculated value at point I, and σ is the standard deviation.

In our study, we tried to match the pressures in **Table A.3.**

TABLE A.3 – OBSERVED AVERAGE BLOCK PRESSURES, SAN JUAN RESERVOIR

# pressure point	Time, days	Pressure, psia
1	0	4679
2	3014	3788
3	3226	3606
4	4171	3979
5	4171	3984
6	4171	3736
7	5966	3575
8	10135	2396
9	10135	2079
10	10135	2476

To achieve a good history match in our single cell model, we adjusted only the pore volume (**Table A.4).**

TABLE A.4 – MODIFIER INFORMATION FOR PARAMETER TO BE CHANGED

Parameter	Modifier action	Modifier	Min. modifier	Max. modifier
Pore Volume	Multiplication	0.9	0.5	1.2

From automatic history match regression, modifying the pore volume within the limits in Table A.4 led to a good match of the observed pressure data. A check of the available petrophysical and geological data suggested a sound geological basis for the changes.

Matches of average static bottomhole pressure and total oil rate are shown in **Figs. A.5** and **A.6.**

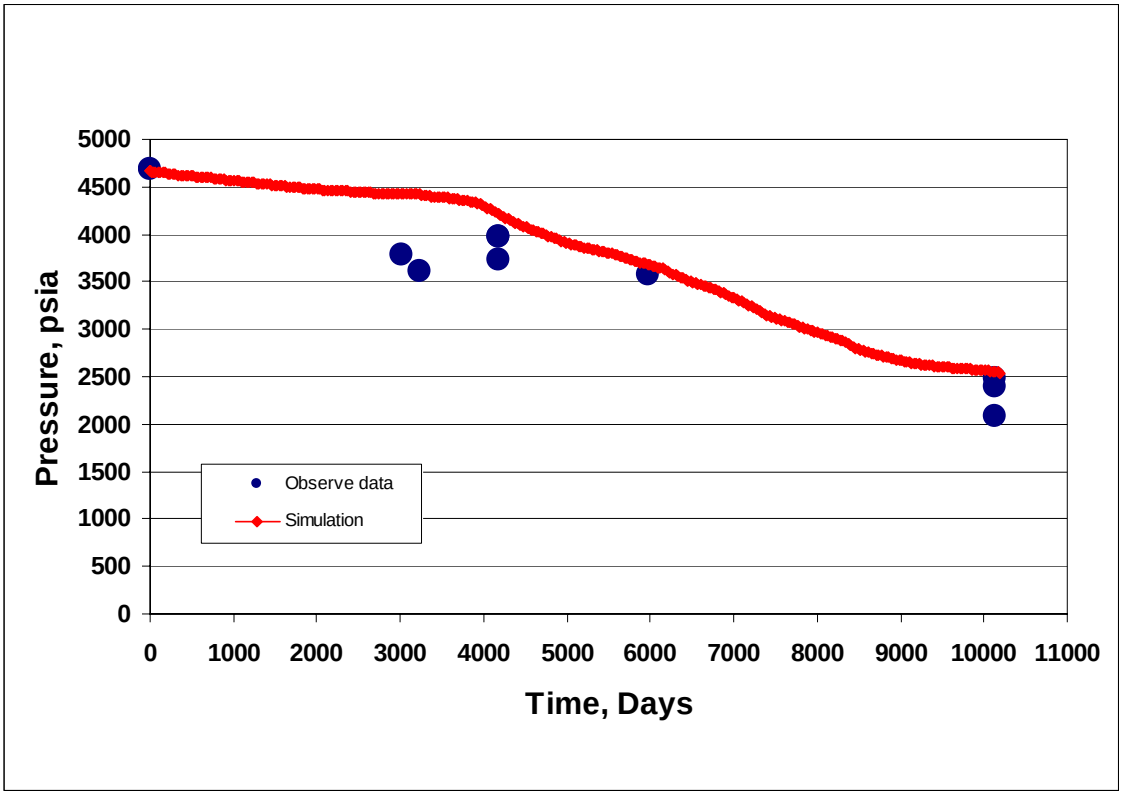

Fig. A.5 – Observed bottom-hole pressures and simulated average pressure in single cell model.

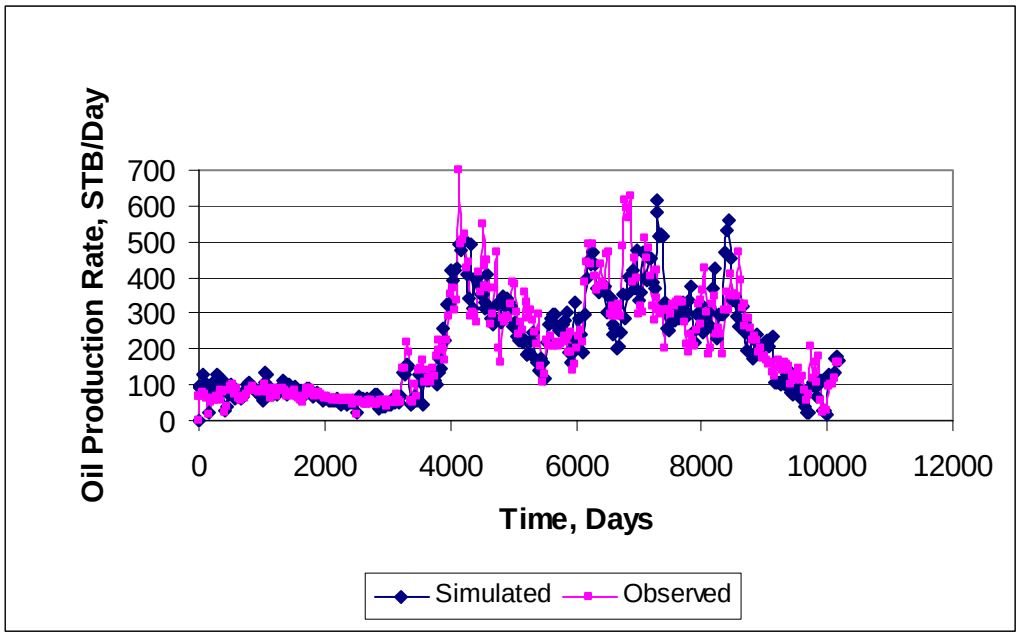

Fig. A.6 – Oil production rate – simulated and observed values.

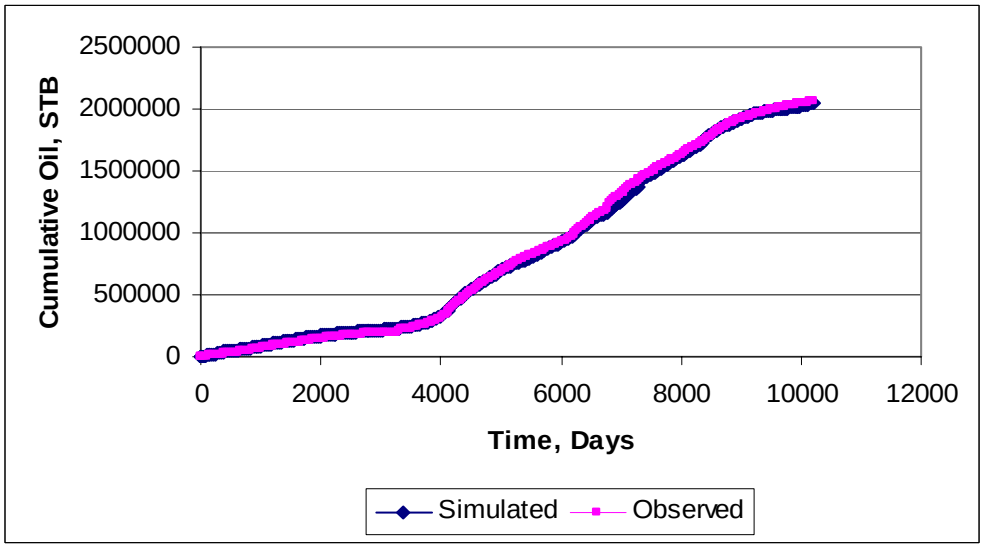

Fig. A.7 – Cumulative oil production – simulated and observed values.

Multi-Cell Model

Another objective of this research was to generated a calibrated reservoir model which could be uses as a tool to evaluate different reservoir manager strategies. Following the material balance and single-cell modeling efforts, we built a 61 x 51 x 3 multi-cell model with 7,144 active cells. Fig. A.8 is a top-of-structure map of the model.

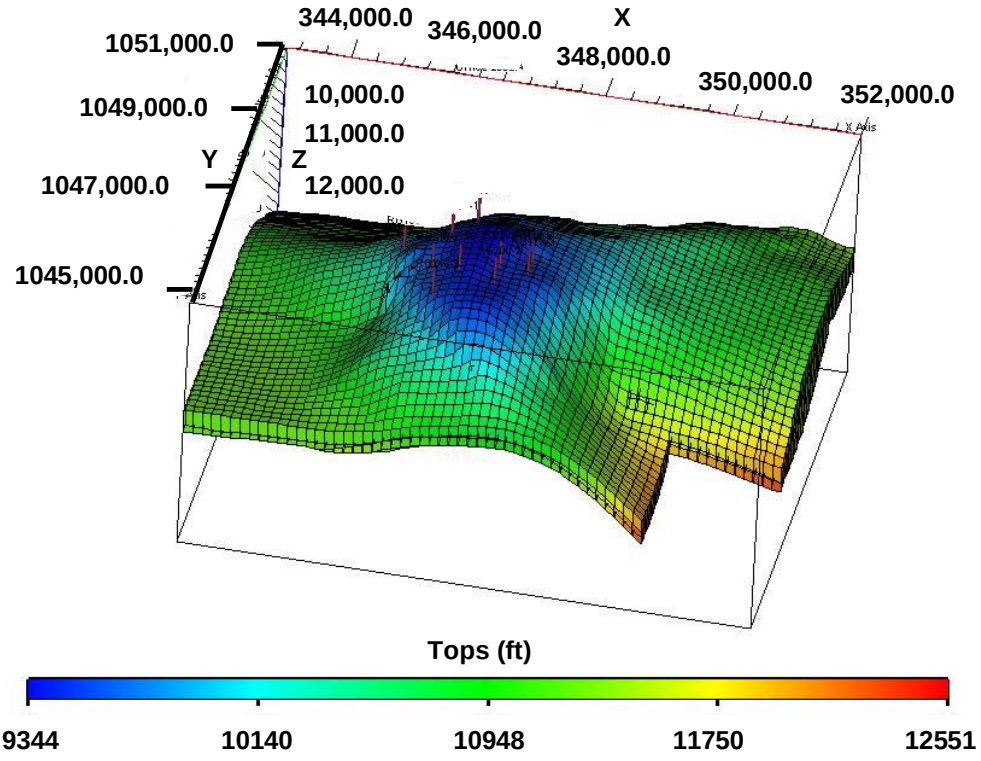

Fig. A.8 –Top of structure, 61 x 51 x 3 cell model of San Juan Reservoir.

Production Data Multi-Cell Model

Extensive production data was collected from PDVSA. The production reports contained monthly cumulative oil, water and gas production for each individual well that was drilled and put on production since the field was discovered in 1973. After 9,000 days of production, oil (condensate) and gas rates have declined steadily, largely because some wells have been shut in (**Fig. A.9)**. After 10,000 days of production, cumulative oil (condensate) and gas production have reached 1.37 $x10^8$ MSCF and $2.10x10^6$ STB, respectively **(Fig. A.10**).

The vast amount of data from 28 years of production and 8 wells is plotted in the (**Figs. A.9** and **A.10**).

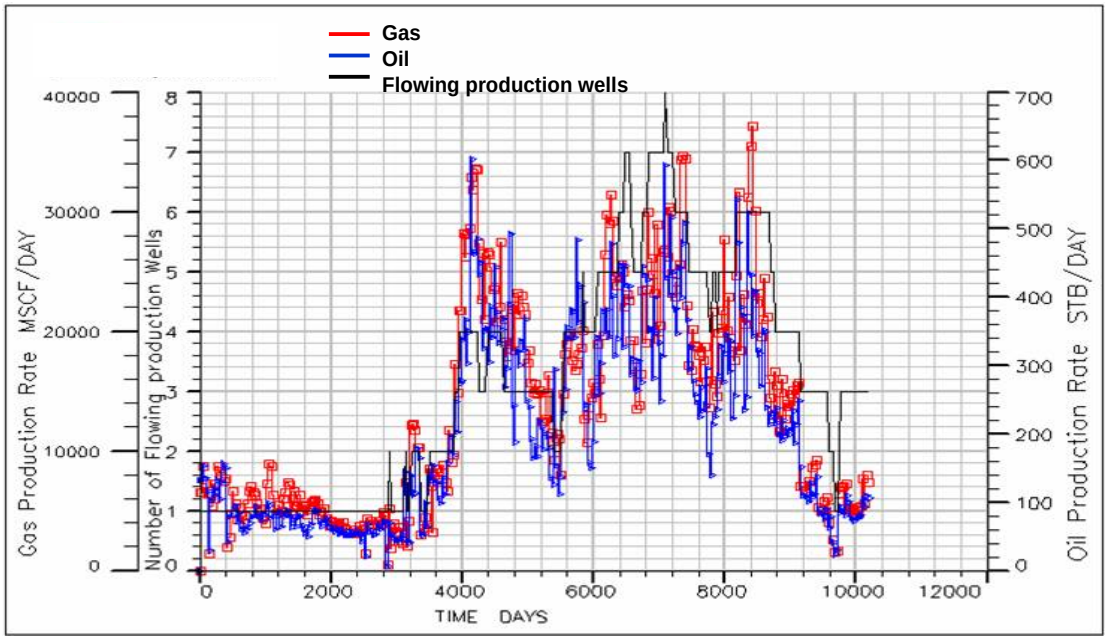

Fig. A.9 – Production rate history of San Juan reservoir, Santa Rosa Field.

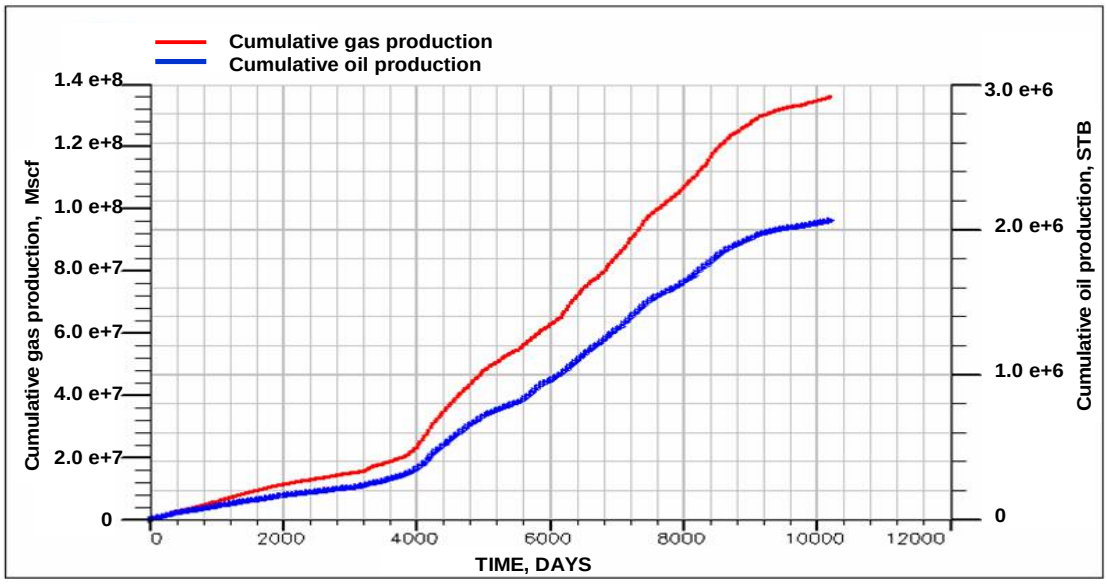

Fig. A.10 – Cumulative production history of San Juan reservoir, Santa Rosa Field.

History Match-Multi-Cell Model

The observed data available consisted of static bottom-hole pressures and water, gas, and oil rates from 1973 to 2001. San Juan experienced numerous mechanical communication problems with other reservoirs, resulting in abnormal water production. The water production reported for the San Juan Reservoir comes mostly from nearby water-bearing sands and water vapor precipitation from gas.

Five mechanical communication problems and one casing failure have been observed.

We matched history using the SIMOPT[12] module of Eclipse, matching static bottom-hole pressures.

The observed data objective function in SIMOPT is the weighted sum of the squares of the mismatch divided by the measurement error, which is expressed as

$$\sum_i \left\{ w_i \times \left(\frac{y_{obs,i} - y_{Calc,i}}{\sigma} \right) \right\}^2 \quad \text{..... (17)}$$

where W_i is weight factor for data point i, $y_{obs,i}$ is observed data point I, $y_{calc,i}$ is calculated value at point I, and σ is the standard deviation.

We attempted to match the pressure in **TABLE A.5.**

TABLE A.5 – OBSERVED AVERAGE BLOCK PRESSURE- SAN JUAN RESERVOIR

Pressure point number	Time, days	Pressure, psia
1	0	4679
2	3014	3788
3	3226	3606
4	4171	3979
5	4171	3984
6	4171	3736
7	5966	3575
8	10135	2396
9	10135	2079
10	10135	2476

To achieve a good history match, the adjustable parameters were pore volume and permeability (**TABLE A.6)**.

TABLE A.6 – MODIFIER INFORMATION FOR PARAMETERS TO BE CHANGED

Parameter	Modifier action	Modifier	Min. modifier	Max. modifier
Pore Volume	Multiplication	1.0402	0.5	1.2
PermXY	Multiplication	0.017018	0.01	10
PermZ	Multiplication	0.01	0.01	10

We obtained a good match using automatic history match regression and modifying the pore volume and permabilities in the suggested order.

After these modifications were made, we focused on objective function for total field bottom-hole pressures (BHP) (**Fig. A.11**) and oil rates (OPR) (**Fig. A.12).**

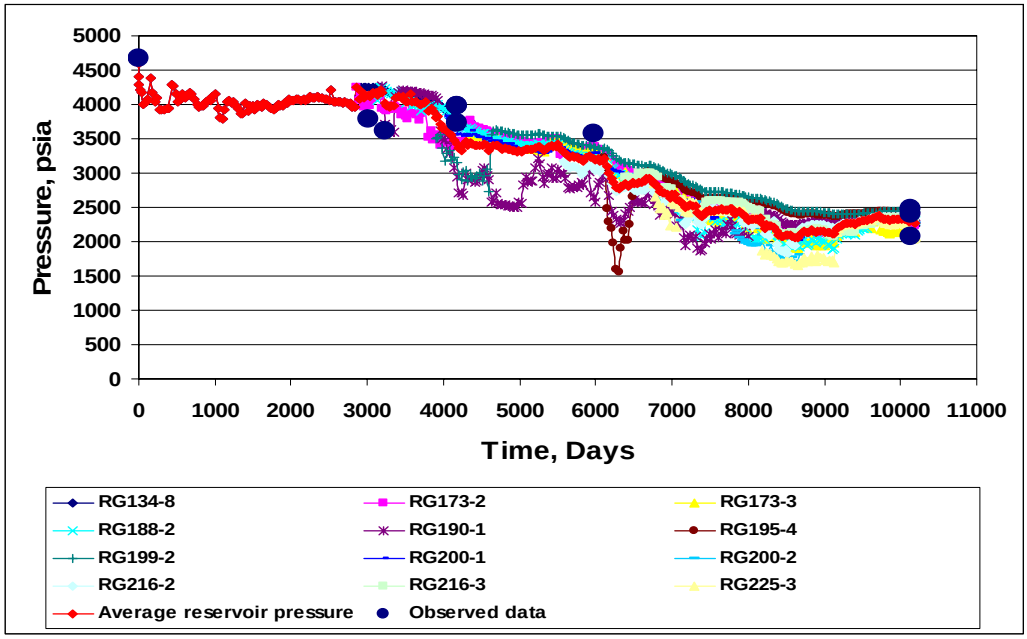

Fig. A.11 – Simulated average and observed bottom-hole pressures.

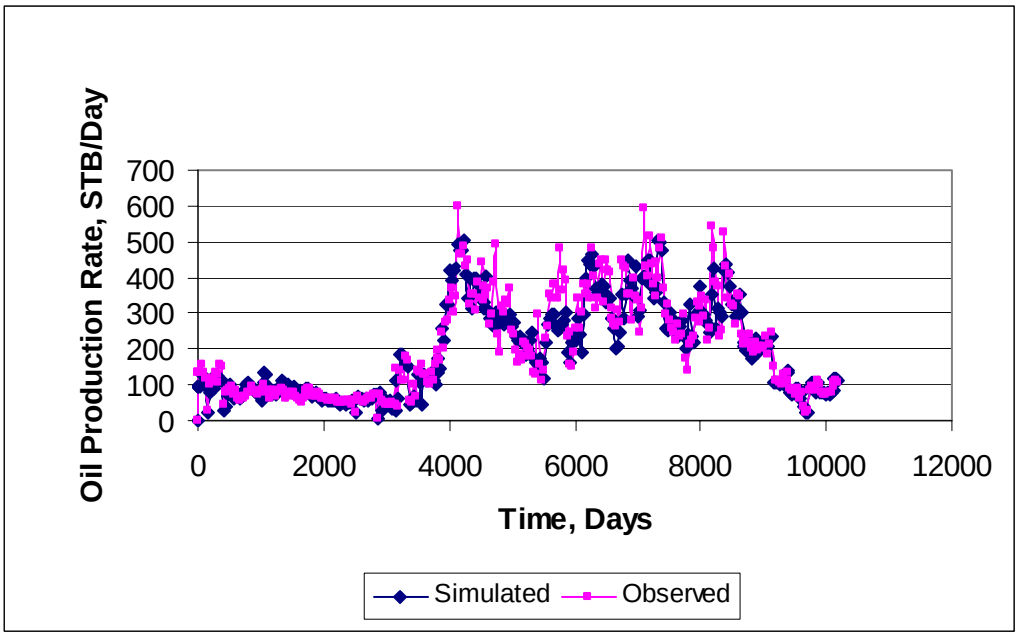

Fig. A.12 – Oil production rate – simulated and observed values.

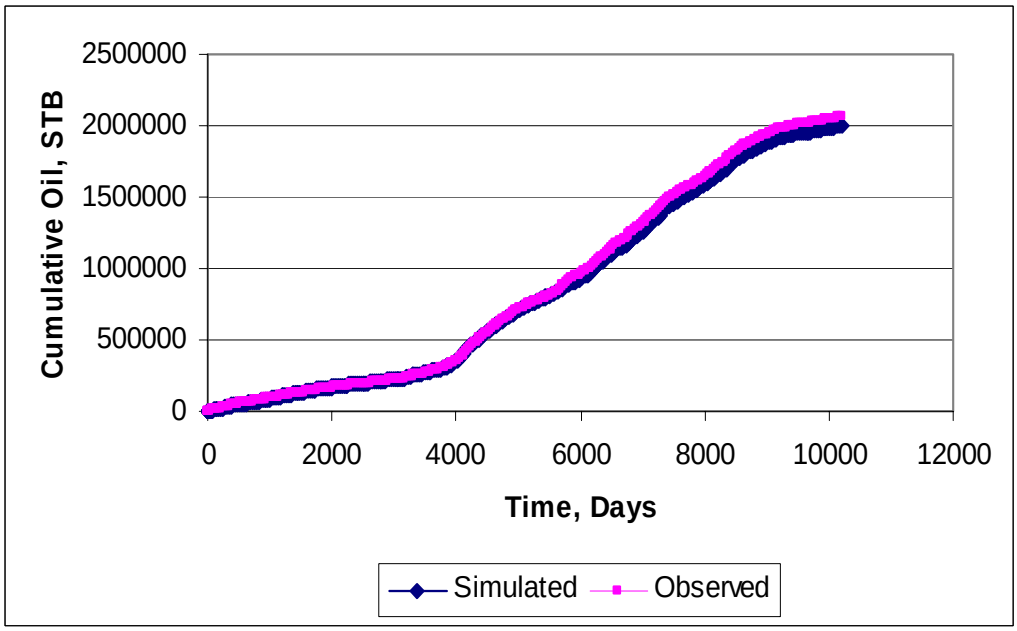

Fig. A.13 – Cumulative oil production – simulated and observed values.

Table A.7 summarizes the estimated ultimate recovery calculated at abandonment pressure of 500 psia from the three different study methods. From table, we can conclude that all of these values of EUR are well within in the range of estimated uncertainty. The results also show that the EUR decrease as we incoroporate more heterogeneities in our models.

TABLE A.7 – EUR FROM THREE DIFFERENT METHODS

Estimated Ultimate Recovery, Mscf		
Material Balance	Single cell	Multicell cell
2.86E+08	2.73E+08	2.69E+08

Fig. A.14 shows observed and simulated pressures for Well RG134-8. **Figs. A.15** and **A.16** show oil rate comparisons.

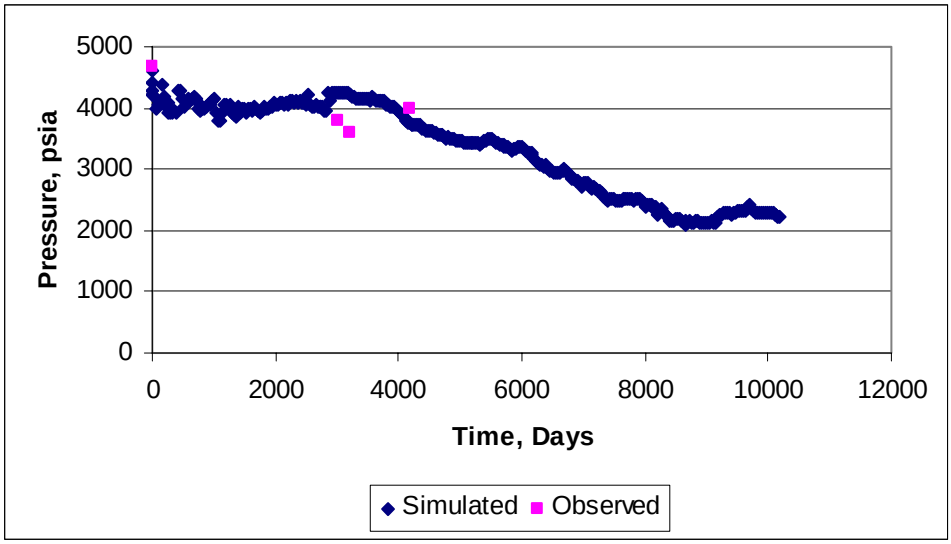

Fig. A.14 – Simulated average pressure and observed bottom-hole pressures–Well RG134-8.

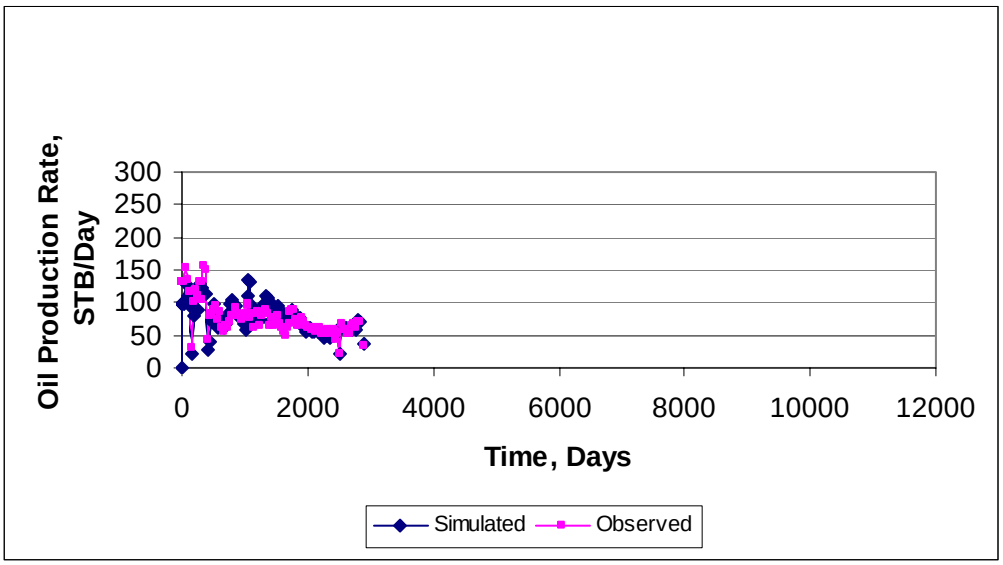

Fig. A.15 – Simulated and observed production rates–Well RG134-8.

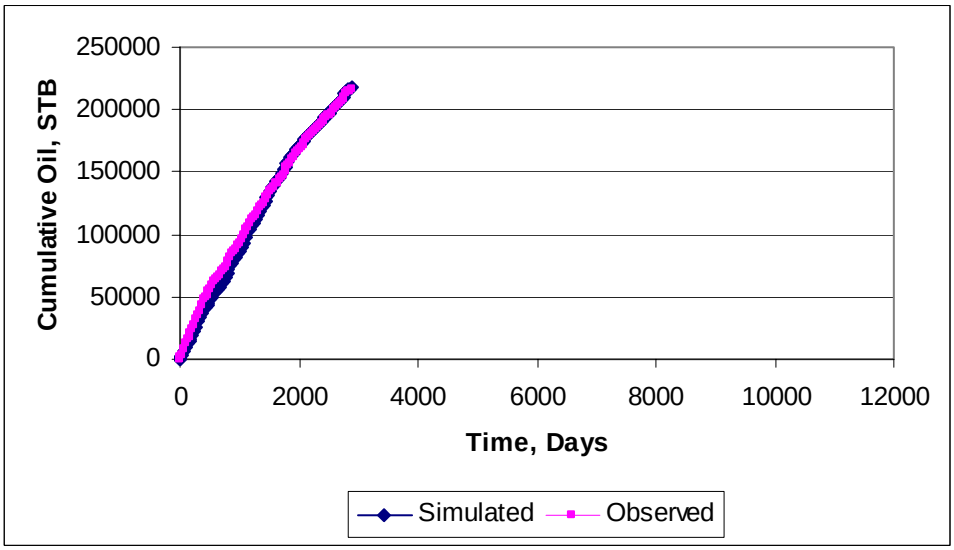

Fig. A.16 – Simulated and observed cumulative oil production – Well RG134-8.

Figs. A.17, A.18, and **A.19** show the results for well RG173-2.

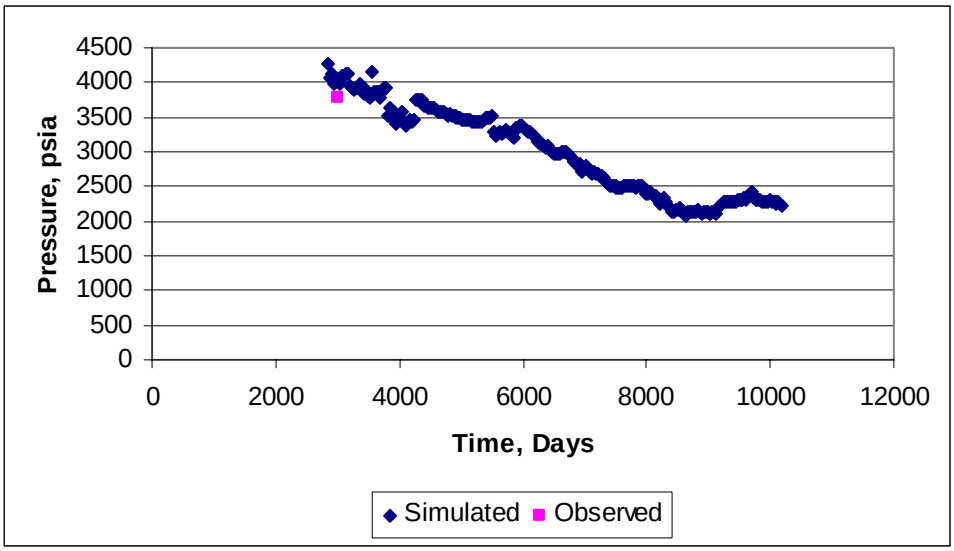

Fig. A.17 – Simulated average and observed bottom-hole pressures- Well RG173-2.

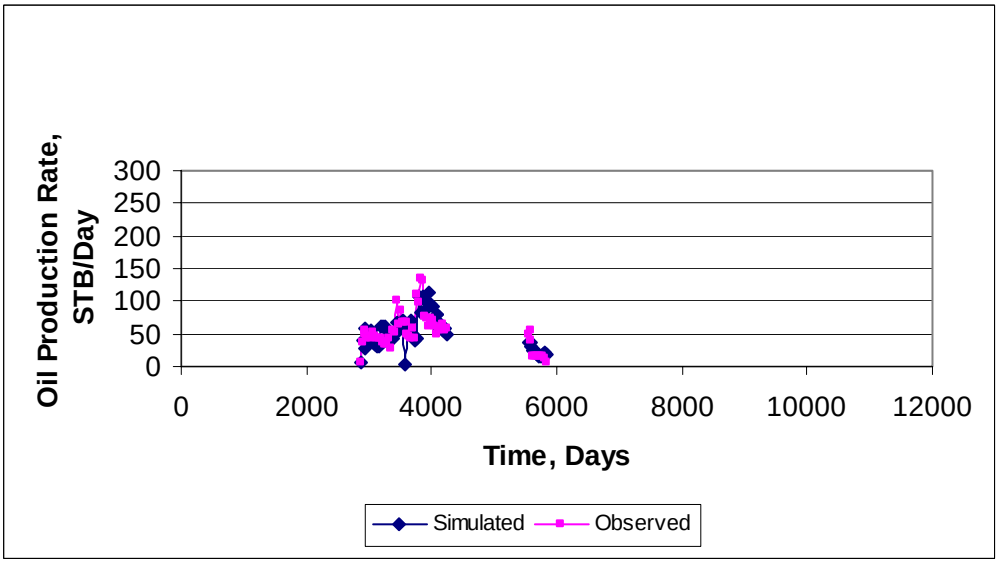

Fig. A.18 – Simulated and observed production rates–Well RG173-2.

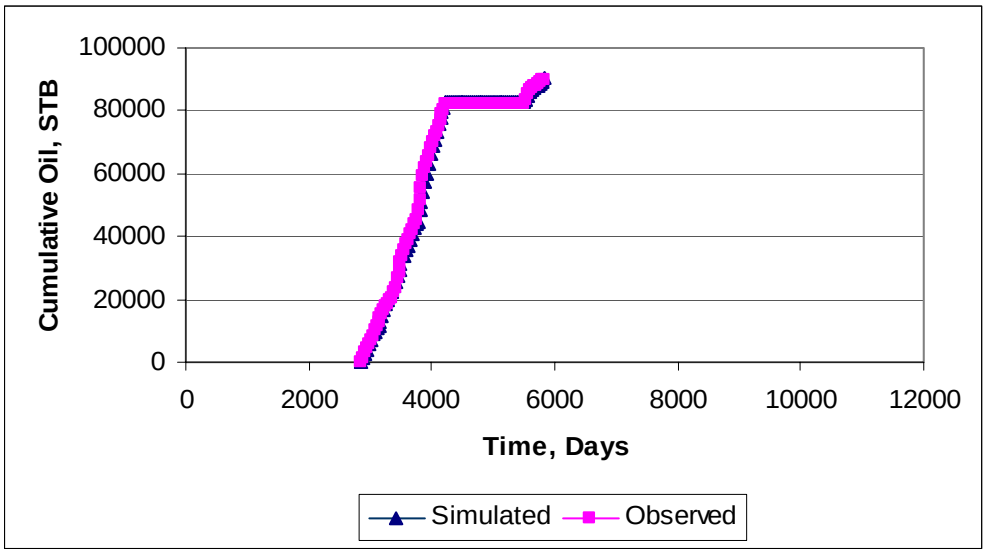

Fig. A.19 – Simulated and observed cumulative oil production – Well RG173-2.

Figs. A.20, A.21, and **A.22** show the results for well RG173-3.

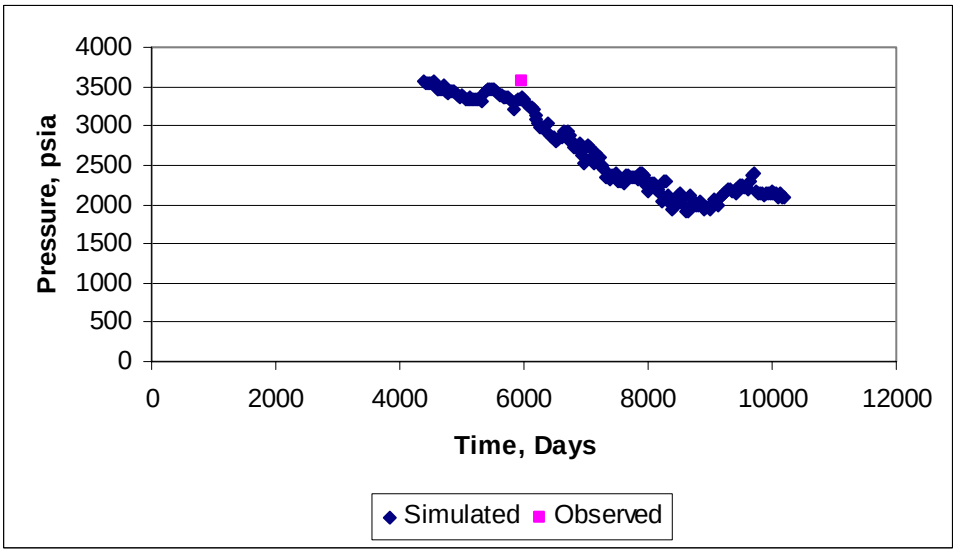

Fig. A.20 – mulated average and observed bottom-hole pressures - Well RG173-3.

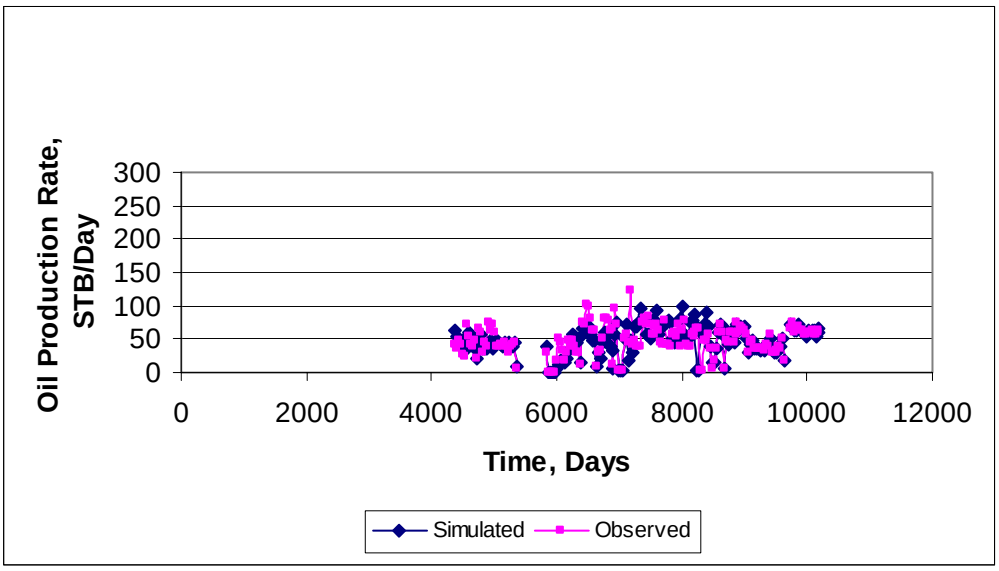

Fig. A.21 – Simulated and observed production rates–Well RG173-3.

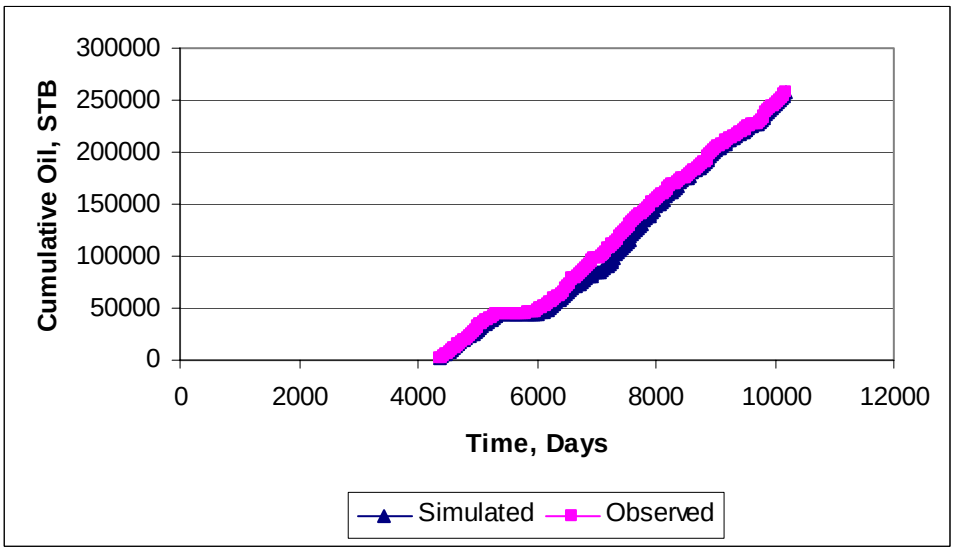

Fig. A.22 – Simulated and observed cumulative oil production – Well RG173-2.

Figs. A.23, A.24, and **A.25** show the results for well RG188-2.

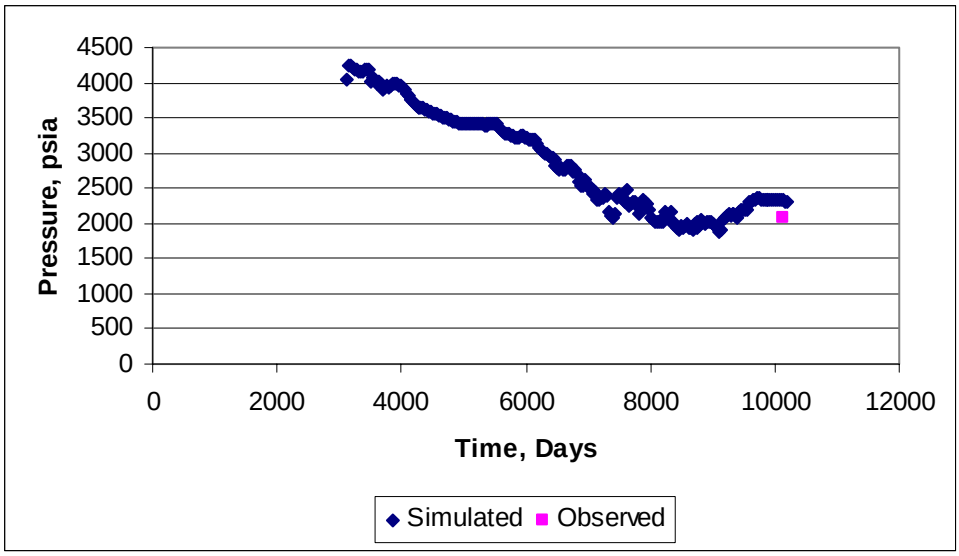

Fig. A.23 – Simulated average and observed bottom-hole pressures - Well RG188-2.

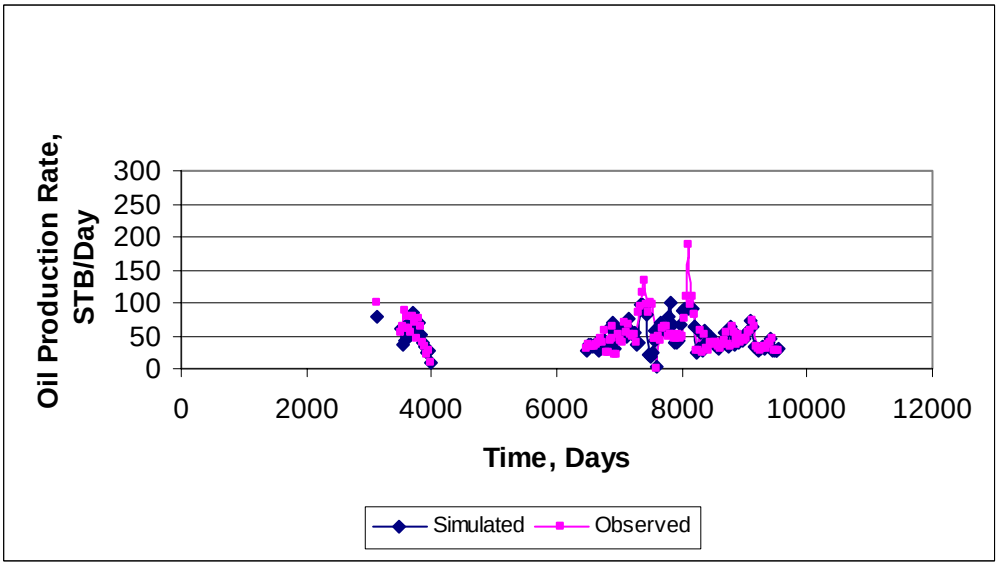

Fig. A.24 – Simulated and observed production rates–Well RG188-2.

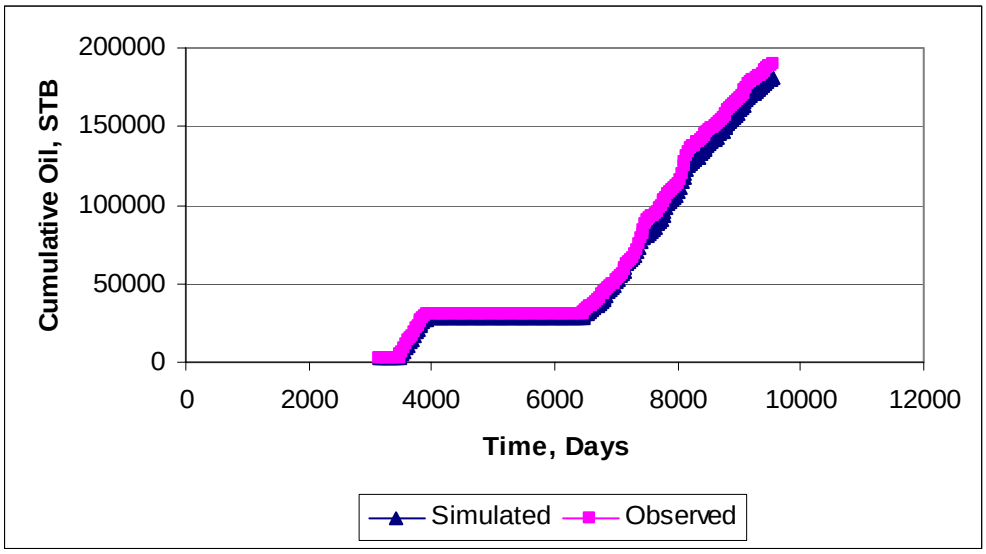

Fig. A.25 – Simulated and observed cumulative oil production – Well RG188-2.

Figs. A.26, A.278, and **A.289** show the results for well RG190-1.

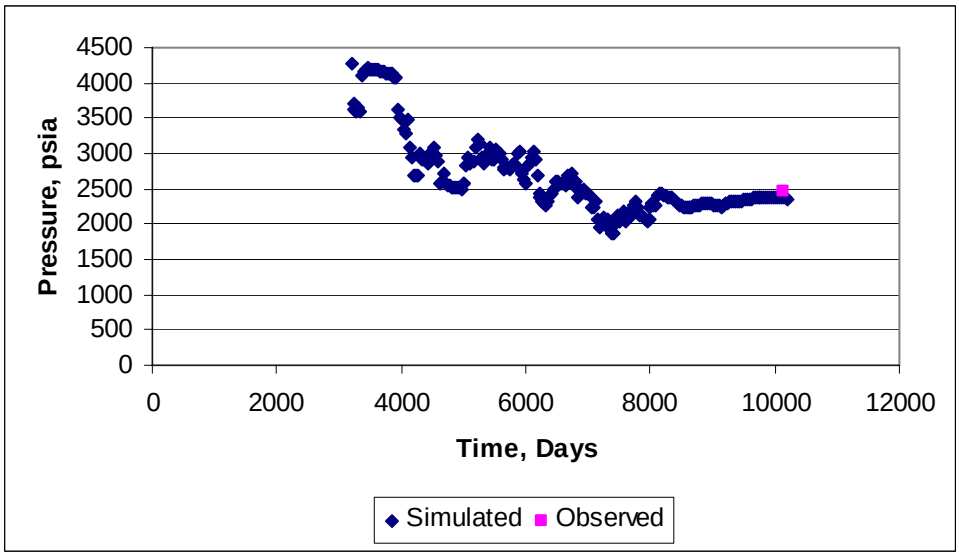

Fig. A.26 –Simulated average and observed bottom-hole pressures - Well RG190-1.

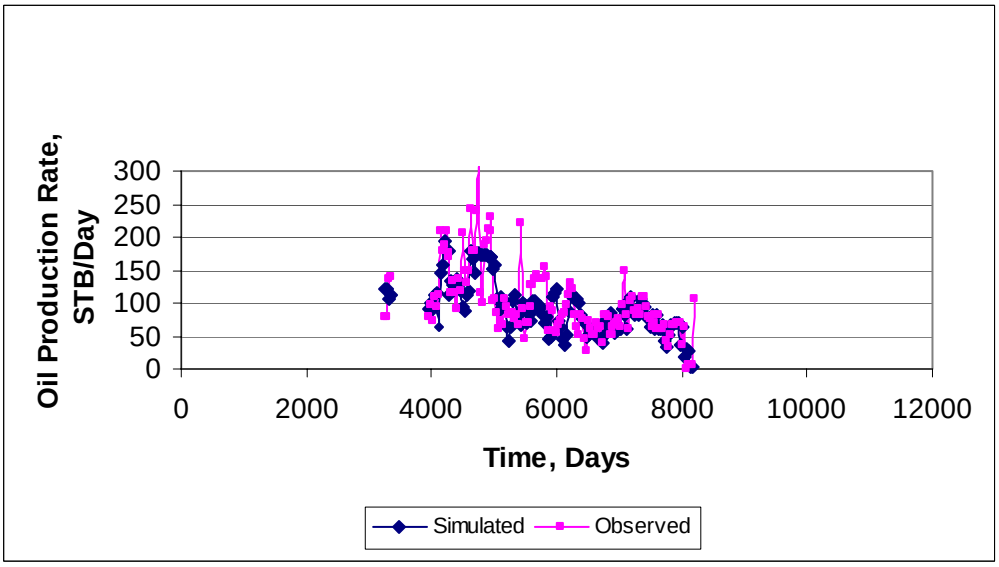

Fig. A.27 – Simulated and observed production rates–Well RG190-1.

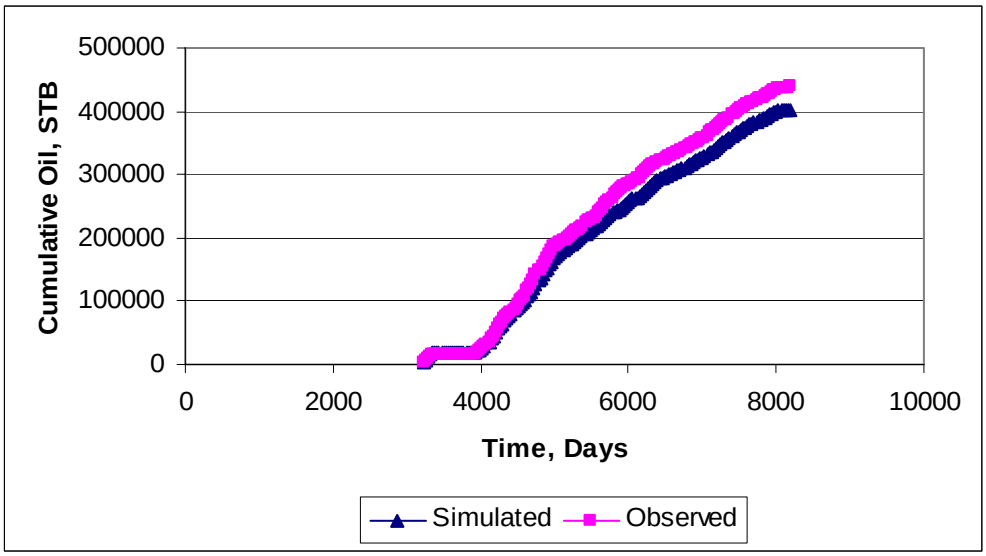

Fig. A.28 – Simulated and observed cumulative oil production – Well RG190-1.

Figs. A.29, A.30, and **A.31** show the results for well RG200-1.

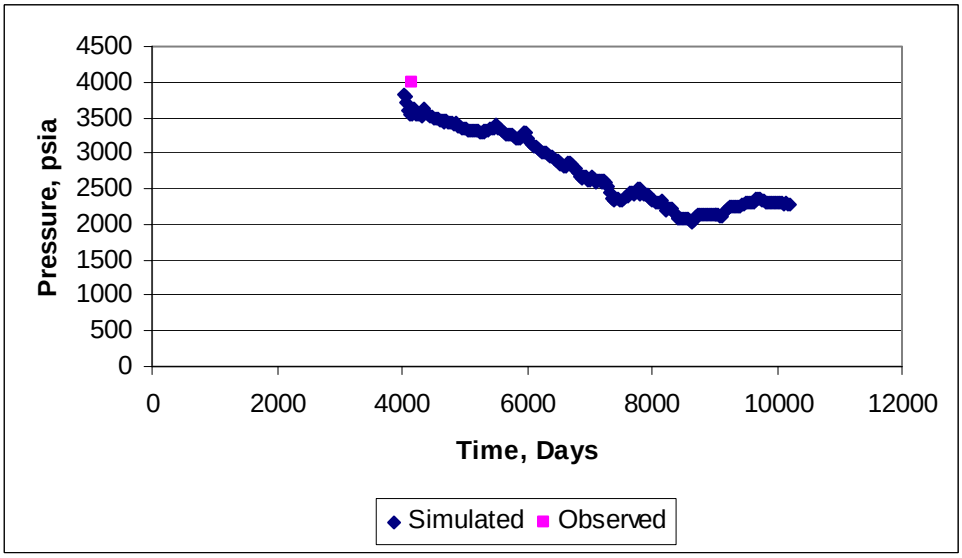

Fig. A.29 –Simulated average and observed bottom-hole pressures - Well RG200-1.

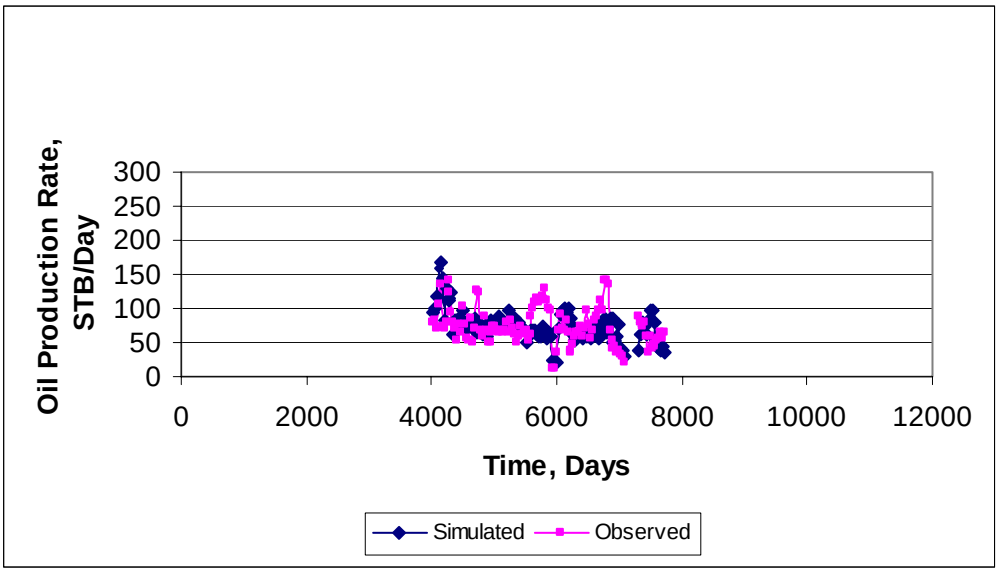

Fig. A.30 – Simulated and observed production rates–Well RG200-1.

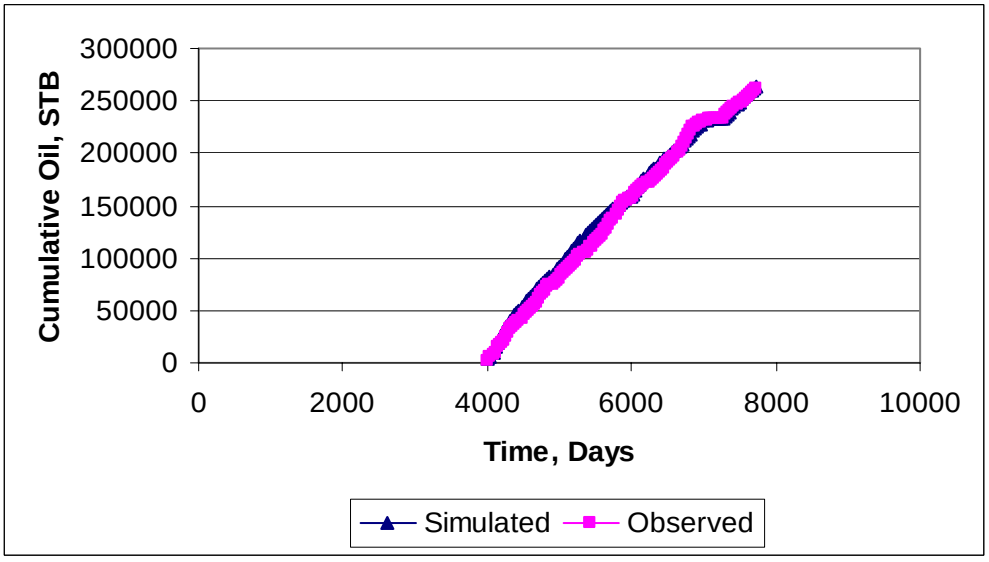

Fig. A.31 – Simulated and observed cumulative oil production – Well RG200-1.

Figs. A.32, A.338, and **A.349** show the results for well RG216-2.

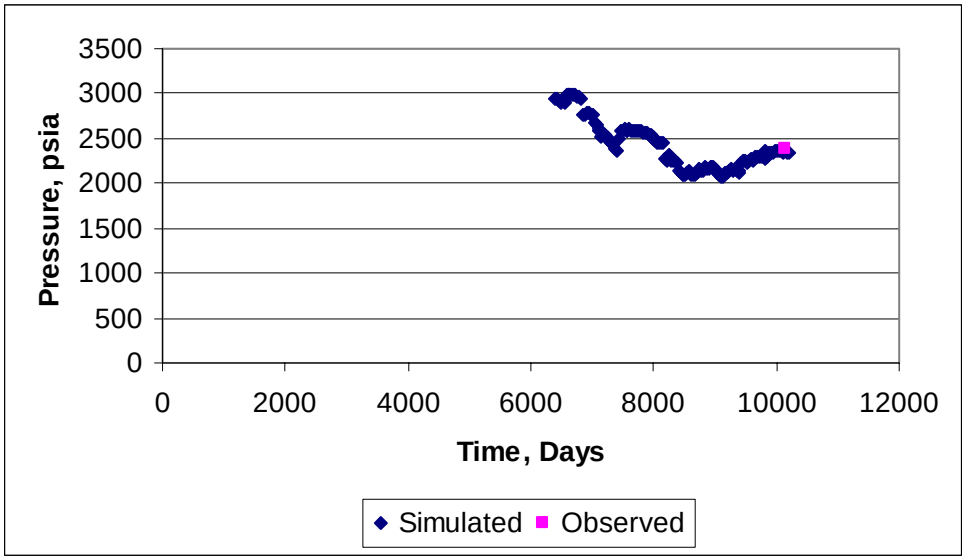

Fig. A.32 – Simulated average and observed bottom-hole pressures - Well RG216-2.

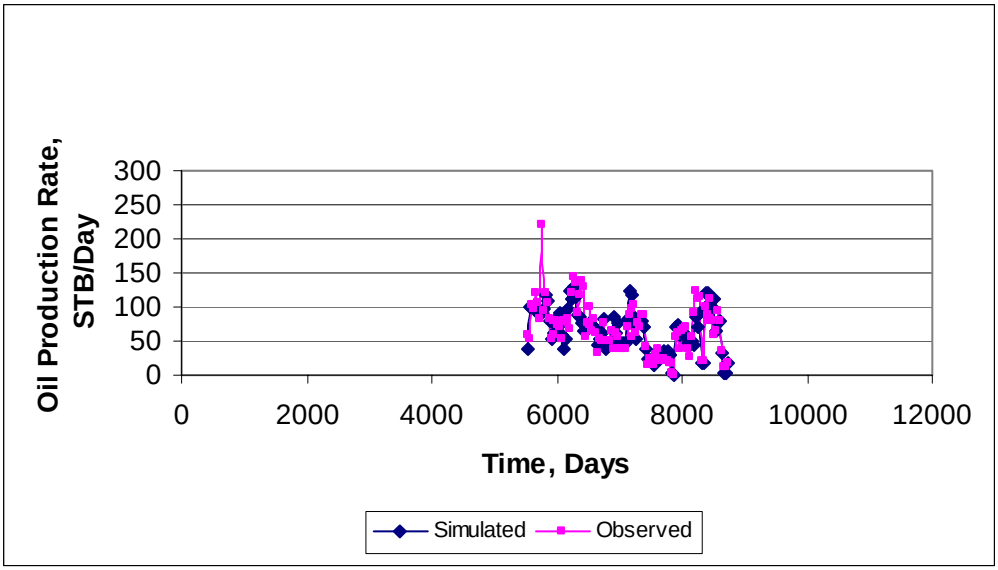

Fig. A.33 – Simulated and observed production rates–Well RG216-2.

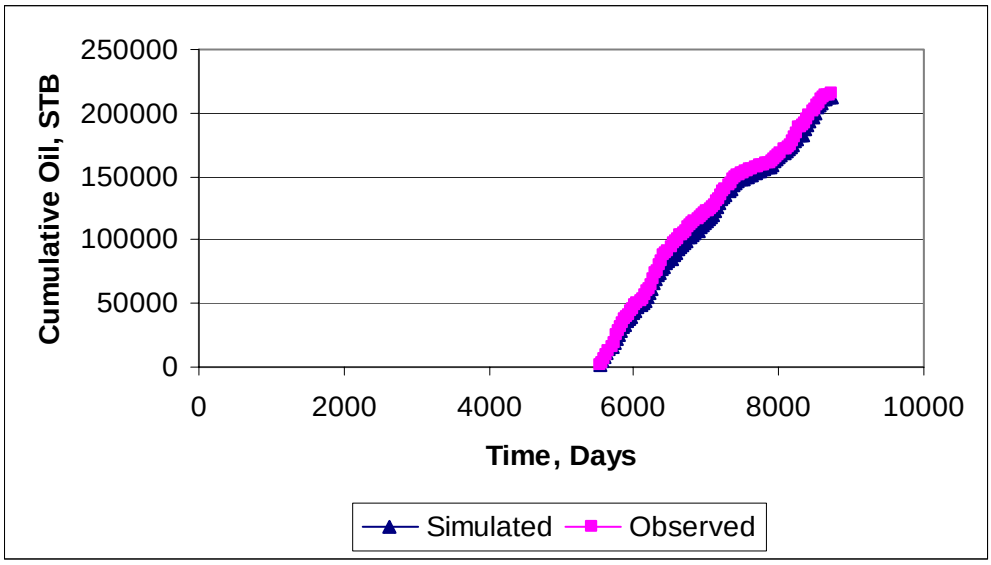

Fig. A.34 – Simulated and observed cumulative oil production – Well RG216-2.

VITA

Name:	Ernesto José Becerra
Born:	January 13, 1966 Barinas, Estado Barinas - Venezuela
Permanent Address:	Alto Barinas Norte, Avenida los Marquitos, CR los Mangos, Calle 5D Casa # 26, Barinas, Estado Barinas – Venezuela. Phone number: (58) 273-5524669
Education:	B.S. Geologist Engineering (May 1991) Universidad de Los Andes, Mérida, Estado Mérida - Venezuela M.S. Petroleum Engineering (December 2003) Texas A&M University, College Station, Texas – USA
Professional Affiliations:	Colegio de Ingenieros de Venezuela Society of Geologist Engineers of Venezuela Society of Petroleum Engineers Venezuelan Student Association – Texas A&M University
Professional Experience:	Petróleos de Venezuela S.A., Reservoir Engineer (1991-2001)